Improving the spin-up of regional EnKF for typhoon assimilation and forecasting with Typhoon Sinlaku (2008)

Shu-Chih Yang[1*], Kuan-Jen Lin[1], Takemasa Miyoshi[2,3] and Eugenia Kalnay[2]

1: Department of Atmospheric Sciences, National Central University
2: Department of Atmospheric and Oceanic Science, University of Maryland
3: RIKEN Advanced Institute for Computational Science, Kobe, Japan

Abstract

The Running-In-Place (RIP) method is implemented in the framework of the Local Ensemble Transform Kalman Filter (LETKF) coupled with the Weather Research and Forecasting (WRF) model. RIP aims at accelerating the spin-up of the regional LETKF system when the WRF ensemble is initialized from a global analysis, which is obtained at coarser resolution and lacks features related to the underlying mesoscale evolution. The RIP method is further proposed as an outer-loop scheme to improve the nonlinear evolution of the ensemble when the characteristics of the error statics change rapidly owing to strong nonlinear dynamics. The impact of using RIP as an outer-loop for the WRF-LETKF system is evaluated for typhoon assimilation and prediction with Typhoon Sinlaku (2008) as a case study.

For forecasts beyond one day, the typhoon track prediction is significantly improved after RIP is applied, especially during the spin-up period of the LETKF assimilation when Sinlaku is developing rapidly from a severe tropical storm to a typhoon. The impact of the dropsondes is significantly increased by RIP at early assimilation cycles. Results suggest that these improvements are because of the positive impact on the environmental condition of the typhoon. Results also suggest that using the RIP scheme adaptively allows RIP to be used as an outer-loop for the WRF-LETKF with further improvements.

1. Introduction

During the last decade, the regional Ensemble Kalman Filter (EnKF) has become an important approach for studying mesoscale instabilities and severe weather prediction. The main advantage of EnKF is the use of the flow-dependent background error covariance, which naturally takes into account the varying dynamical instabilities and topography, in comparison with the static error covariance used in the three-dimensional variational analysis (3DVar) method; another common assimilation method used in many operational centers. In EnKFs, the accuracy of the ensemble mean state is important for determining the dynamical evolution of the ensemble, and the flow-dependent errors carried in the ensemble perturbations are essential in providing effective analysis corrections. Thus, both the accuracy of the mean state and the structure of the ensemble perturbations are key factors in the good performance of EnKFs. An EnKF reaches its asymptotic performance after the ensemble represents a reasonable sample of the background error statistics. For this reason, EnKFs require a spin-up period of sufficient time to accumulate enough observation information (Caya et al. 2005). Also, the way in which the ensemble of an EnKF is initialized has a strong impact on the length of spin-up (Kalnay and Yang 2010). Furthermore, due to the Gaussian assumption for the ensemble distribution, the EnKF's performance is limited by strong nonlinearity, arising from infrequent or sparse observations, poor initial ensemble members, and strong nonlinear dynamics (Lawson 2004). Among these causes, highly nonlinear dynamics modify abruptly the dynamically related (background) errors and may lead towards filter divergence.

For regional EnKFs, the initial ensemble is usually "cold-started" when a case of interest, such as tropical cyclones (TCs) or mesoscale convection systems, emerges. The initial ensemble is usually centered on the operational global analysis and the ensemble perturbations are selected randomly (Torn et al. 2006). As neither this initial mean state nor the set of perturbations is optimal for mesoscale features, this introduces an inevitable long spin-up in the process of developing dynamically relevant ensemble perturbations. Therefore, it is usually recommended to have at least a three-day spin-up period to derive reliable regional EnKF analyses. However, such initialization introduces serious difficulties if waiting longer than the spin-up period is not an option for the forecasters. For example, when predicting a rapidly developing/intensifying tropical storm or dealing with a fast moving, short-lived mesoscale weather event. Also, considering that limited observations are available over open water, the spin-up required for typhoon assimilation and prediction might be even longer in order to accumulate sufficient information about the system. Dirren et al. (2007) suggest that initializing the ensemble from a larger ensemble mean error and

spread allows the regional EnKF system to spin-up more quickly, which could alleviate the issue of an under-dispersive spread. Thus, the initial ensemble is centered at a long-hour forecast (48-h NCEP GFS forecast) and the amplitude of the ensemble perturbations needs to be artificially amplified. This setup, also used in Torn et al. (2011), is designed to "inflate" the initial background error covariance in order to emphasize the contribution from observations, but it neglects the fact that the structure of the ensemble-based error covariance could still represent poorly the underlying dynamical uncertainties. For typhoon prediction, the spin-up of regional EnKFs becomes even more critical because during the spin-up period, tropical cyclones are developing over open waters, where observations are valuable, but rather limited in number. Observations, such as those obtained by reconnaissance aircraft (Wu et al. 2005) cannot be effectively assimilated with a less optimized background error covariance during the spin-up, and forecasts are only initiated after the completion of the EnKFs spin-up (Torn et al. 2011; Kunii et al. 2012). Moreover, on average it takes only 4.8 days for a tropical depression formed over the Northwest Pacific to develop into a tropical cyclone (TC) and to approach and even make landfall on the island of Taiwan. Therefore, improving the forecast performance at the early development stage of typhoons becomes an important task for Taiwan in order to gain sufficient time for disaster protection. Moreover, severe weather events could involve very strong nonlinear dynamics and limit the performance of the EnKF. For example, typhoons might undergo rapid intensification through thermodynamical effects or air-sea interaction (Lin et al. 2005). Also, large uncertainties about the track arise when TCs interact with the monsoon trough causing an abrupt northward turn (Lander 1996), or when they become embedded in a saddle field with strong uncertainties over the steering flow (Wu et al. 2004). The issue of nonlinearity becomes even more complicated with infrequent or sparse distribution of observations. If the ensemble does not capture such abrupt changes in the background dynamics, assimilation of observations cannot be effective with this less-optimal ensemble-based error covariance. Also, if the ensemble space is under-dispersive, filter divergence might occur. In order to address these concerns, it is clear that under such circumstances the ensemble needs to be "spun-up" again to catch up the true dynamics.

The "Running In Place (RIP)" method was proposed by Kalnay and Yang (2010; hereafter KY10) in order to deal with the spin-up issues of EnKF and is implemented within the framework of the Local Ensemble Transform Kalman Filter (LETKF). The RIP method is intended to improve both the accuracy of the mean state and the flow-dependent structure of the error covariance, such that the spin-up could be accelerated. With a simple dynamical quasi-geostrophic (QG) model, KY10 demonstrated that the RIP method could successfully

shorten the LETKF's spin-up to a period comparable with 4DVAR, which originally had the shortest spin-up among the assimilation schemes implemented in the QG model. Most importantly, the accuracy of the EnKF analysis can still be maintained after the spin-up. Furthermore, given that the error statistics could change abruptly when the underlying flow undergoes highly nonlinear dynamics, which could lead to filter divergence, Yang et al. (2012a; hereafter YKH12) proposed that the RIP method could be served as a generalized outer-loop for the EnKF framework, in order to improve the nonlinear evolution of the ensemble. As a proof of concept, this study was carried out with the Lorenz three-variable model under the perfect model assumption. With RIP, filter divergence could successfully be avoided and the analysis accuracy using a longer assimilation window is significantly improved upon the standard LETKF. As RIP uses observations N times, the ensemble spread is reduced by the order $\sqrt{N}$, and the smaller corrections allow the increments to follow the nonlinear path towards the truth better than with a single increment. By improving the nonlinear evolution of the ensemble, the ensemble space for correction is better represented.

Yang et al. (2012b; hereafter Y12b) further investigated applications with the RIP method using the Weather Research and Forecasting (WRF) model coupled with the Local Ensemble Transform Kalman Filter (LETKF) data assimilation system. This system was applied to typhoon assimilation and prediction under an observation simulation system experiment (OSSE) framework. The OSSE experiments showed that the RIP method is able to accelerate the dynamical adjustment of the typhoon structure during the LETKF spin-up period (defined as the first two days of the assimilation experiment) and improves both the accuracy of the mean state and the flow-dependent structure of the ensemble-based error covariance. The improvements included not only the inner-core of the typhoon structure, but also the environmental conditions for the typhoon movement. As a result, the LETKF-RIP analysis leads to better typhoon prediction, capturing the change of the typhoon track 12 hours earlier than provided by the standard LETKF analyses. Recently, Wang et al. (2012) implemented a similar idea to the RIP method in the WRF-Ensemble Square Root filter system (the iterative EnSRF) to spin-up the radar data assimilation for an idealized supercell storm under an OSSE framework. Their results also confirm that the iterative EnSRF can accelerate EnSRF to reach a steady level of state estimation. Also, better performance of the iterative EnSRF is obtained because of the improved background error covariance and accuracy of the mean state. More importantly, the correlations between the observed and unobserved variables are improved through the iterative EnSRF iterations.

This study further investigated the impact of the RIP method on real observations from the 2008 Typhoon Sinlaku, using the WRF-LETKF system. We note that this is the first NWP application where RIP is applied in a real case of typhoon assimilation and prediction. In 2008, valuable dropsonde data were obtained in the THORPEX Pacific Asian Regional Campaign (T-PARC; Elsberry and Harr 2008), and Typhoon Sinlaku is the one that was most thoroughly observed throughout its lifetime. The main motivation of this study is to explore whether these valuable dropsondes could have be used more effectively by the RIP method during the early developing stage of Sinlaku.

We note that many studies were made to highlight the impact of the T-PARC dropsondes for typhoon prediction (Aberson 2003; 2011; Wu et al. 2007; Chou et al. 2011; Harnisch and Weissmann 2010; Weissmann et al. 2011). Weissmann et al. (2011) compared the results of assimilating the dropsonde data during the T-PARC period with four different models (ECMWF, JMA, NCEP, and WRF). Chou et al. (2011) evaluated the improvement on the TC track forecast derived by assimilating the dropsonde data in the DOTSTAR and T-PARC projects with the NCEP global forecast system (GFS). Both studies have shown that after assimilating the dropsonde data, the TC track forecast could be significantly improved. Wu et al. (2012a) investigated the steering flow from the results of Chou et al. (2011). They concluded that the primary benefit from assimilating dropsondes for Sinlaku was to improve the vertical vortex structure that extends further into the troposphere; therefore, the typhoon could be advected by a more representative steering flow in the deep troposphere. As we will demonstrate in Section 4, the dropsonde data during early assimilation cycles could be used significantly more effectively with the RIP method. Thus, through the case study of the well-observed typhoon Sinlaku, we will show that RIP using real observations is able to improve the performance of the WRF-LETKF system during its spin-up time and thus, improve the effectiveness of the observations. Moreover, we explore the possibility of using RIP as a generalized outer-loop in the WRF-LETKF framework, as proposed in YKH12.

This paper is organized as follows. In Section 2, the 2008 Typhoon Sinlaku is described briefly. Section 3 introduces the WRF-LETKF system and discusses the implementation of the RIP method. Results of the assimilation experiments are presented in section 4, and finally, Section 5 gives the summary and conclusions.

2. Typhoon Sinlaku (2008-09-09 ~ 2008-09-21)

Typhoon Sinlaku formed at 1800 UTC on 8 September 2008 on the east side of the Philippines and it then moved north-northwest. Figure 1 shows the best track and the

intensity of Sinlaku, which was analyzed by the Joint Typhoon Warning Center (JTWC). During 9–10 September, Sinlaku intensified rapidly with its maximum wind speed increasing from 65 to 110 kts, reaching its highest value of 125 kts at 1800 UTC on 11 September, and reaching its lowest sea level pressure of 925 hPa at 0600 UTC on 11 September. Sinlaku is characterized by a meandering track. During its intensifying period, Sinlaku continued moving slowly northwards (~1.9 m/s) associated with the saddle field formed between the subtropical and continental high pressure systems. About 12 September, due to the westward expansion of the subtropical high, Sinlaku turned to move northwestwards toward Taiwan. At daybreak of 14 September, Sinlaku landed at Ilan, the northeastern tip of Taiwan and then continued moving northwestwards. After it moved away from Taiwan and entered the Taiwan Strait at 1800 UTC 14 September, the extension of the subtropical high decreased and Sinlaku gradually crossed the ridge of the subtropical high and started to move northeastwards. After that, Sinlaku was influenced by the mid-latitude westerlies and continued moving northeastwards, passing the southern ocean of Japan. At the end of its life cycle, it underwent a subtropical transition and turned into a subtropical cyclone on 21 September.

Typhoon Sinlaku is the most observed case during the T-PARC period, especially with regard to dropsonde observations. The dropsonde distribution at different times is shown in Figure 2. The life cycle of Sinlaku is full of many important and distinctive features of typhoons, including: the rapidly intensifying stage, the mature stage, (double) eyewall reconstruction, and the dissipation stage influenced by an ocean cold eddy, and its subsequent transformation into a subtropical cyclone. These valuable observations provide a great opportunity to improve our understanding of typhoons at different stages. As a result, Sinlaku has been widely studied for topics related to typhoon dynamics (Huang et al. 2012; Wu et al. 2012b), model simulation (Weissmann et al. 2011; Chou et al. 2011), regional data assimilation (Miyoshi et al. 2011), and observation impact estimation (Kunii et al. 2012).

As Chou et al. (2011) and Wu et al. (2012a) noted, the forecast tracks for Sinlaku from the ensemble prediction system using global models show large spread and uncertainties when the typhoon moved slowly to the southeast of Taiwan, during late 10 September to 11 September. The complexity of the large-scale environmental flow in the vicinity of Sinlaku caused the meandering motion and poor skill in representing these synoptic features in the global models is one of the primary causes of large errors in the forecast track.

3. Model and assimilation system

3.1 The "Running-In-Place" (RIP) method in the LETKF framework

As indicated above, the RIP scheme was proposed by KY10 in order to accelerate the spin-up period of an EnKF when initializing the assimilation from a state far from the true dynamics (e.g., a cold start), or when the background error statistics suddenly change (e.g., a rapid regime change in the dynamics). With RIP, the accuracy of the mean state and ensemble-based background error covariance are both improved simultaneously to capture the underlying true dynamics, as represented by the observations. Below, RIP is described briefly within the LETKF (Hunt et al. 2007) framework and further details are presented in KY10 and YKH12.

Unlike variational analysis methods (3D/4D-Var), the LETKF belongs to the class of sequential data assimilation that minimizes the analysis error variance. At each analysis grid point, the LETKF performs data assimilation to update both the mean and perturbations of the ensemble, according to the local information of the background (a short-range forecast) and regional observations. In the LETKF, optimal weights for the background ensemble perturbations are derived, so that this linear combination of the ensemble perturbations minimizes the analysis error variance (in the local domain). With K background ensemble members at time t_{n}, the analysis ensemble perturbation (deviations from the ensemble mean) at the analysis time t_n are computed as follows:

$$\mathbf{X}_n^a = \mathbf{X}_n^b \mathbf{W}_n^a \tag{1}$$

Here, $\mathbf{X}_n^b = \left[\delta\mathbf{x}_n^{b,1} \middle| \cdots \middle| \delta\mathbf{x}_n^{b,k} \right]$ is the matrix of the background perturbations whose columns are the vectors of ensemble perturbations that deviate from the ensemble mean: i.e., $\delta\mathbf{x}_n^{b,k} = \mathbf{x}_n^{b,k} - \overline{\mathbf{x}}_n^b$, where $\mathbf{x}_n^{b,k}$ is the k^{th} background ensemble member and $\overline{\mathbf{x}}_n^b$ is the background ensemble mean. Similar definitions are applied to the analysis ensemble mean ($\overline{\mathbf{x}}_n^a$) and perturbations ($\mathbf{X}_n^a$). The analysis perturbation weight matrix $\mathbf{W}_n^a$ is computed by:

$$\mathbf{W}_n^a = \left[(K-1)\hat{\mathbf{P}}_n^a \right]^{1/2}. \tag{2}$$

where $\hat{\mathbf{P}}_n^a$ is the analysis error covariance matrix in the ensemble space, given by:

$$\hat{\mathbf{P}}_n^a = \left[(K-1)\mathbf{I}/\rho + \mathbf{Y}_n^{b\,T} \mathbf{R}^{-1} \mathbf{Y}_n^b \right]^{-1}. \tag{3}$$

Here, $\mathbf{Y}_n^b = \left[\delta\mathbf{y}_n^{b,1} \middle| \cdots \middle| \delta\mathbf{y}_n^{b,k} \right]$ is the matrix of the background ensemble perturbations in

observation space where $\delta \mathbf{y}_n^{b,k} = h(\mathbf{x}_n^{b,k}) - \overline{h(\mathbf{x}_n^b)}$, $\mathbf{R}$ is the observation error covariance matrix, $h(\bullet)$ is the observation operator that converts a variable from model to observation space and ρ is the multiplicative covariance inflation factor. The superscript T in Eq. (3) stands for matrix transpose, and the inflation coefficient ρ is constant throughout the assimilation experiments. We note that adaptively adjusting the inflation factors might improve the overall performance of the LETKF system further (Miyoshi and Kunii 2011; Miyoshi 2011), but a spin-up period is also required with such an adaptive inflation method.

The analysis ensemble mean at time t_n is obtained from

$$\mathbf{x}_n^a = \mathbf{X}_n^b \overline{\mathbf{w}}_n^a + \overline{\mathbf{x}}_n^b , \tag{4}$$

where

$$\overline{\mathbf{w}}_n^a = \hat{\mathbf{P}}_n^a \mathbf{Y}_n^{b\,T} \mathbf{R}^{-1} (\mathbf{y}_n^o - \overline{\mathbf{y}}_n^b) . \tag{5}$$

In Eq. (5), $\mathbf{y}_n^o$ and $\overline{\mathbf{y}}_n^b = \overline{h(\mathbf{x}_n^b)}$ are the column vectors for the observations and the background ensemble mean in observation space, respectively.

Equations (1) to (5) provide the basic formulas of the standard LETKF. Based on the framework of the standard LETKF, the RIP scheme includes a "no-cost" smoother and forward model integrations (KY10). The no-cost smoother is constructed from the weights derived during the LETKF analysis (Eqs (2) and (5)), which linearly combines the background ensemble trajectories in order to minimize the analysis error variance at the analysis time t_n. If perturbations evolve linearly within an assimilation window, the linear combination of the ensemble trajectories approximates a model trajectory; thus, if this trajectory is closest to the truth at the analysis time, and if model errors are small, this trajectory should also be closest to the truth throughout the window. Therefore, the weights obtained at the analysis time should also be valid throughout the assimilation window (KY10). These LETKF weights allow for the construction of a "no-cost" smoother for the LETKF, which improves the model ensemble state at an earlier time using observations that are obtained later within the analysis window, without the need of an adjoint model (Kalnay et al. 2007; Yang et al. 2009, see the footnote 1 in KY10 for detailed explanation for "no-cost"). This is equivalent to an ensemble-based Kalman smoother (Evensen 2003, Appendix D).

The RIP scheme has two steps: (1) the use of the no-cost smoother to update the ensemble states at a time earlier than the current analysis time, and (2) forward integrate these smoothed (and improved) ensemble states to the current analysis time and assimilate the same set of observations. In KY10 and YKH12, these two steps are repeated iteratively for a window between the previous and current analysis times, [t_{n-1}, t_n]. However, with a dynamically complex model such as WRF, the window for applying the no-cost smoother becomes shorter than the analysis interval, given the nonlinearity of the mesoscale dynamics. Therefore, Y12b modified the implementation in order to optimize the use of the RIP method with WRF for a 6-h analysis cycle and with two loops are adopted (see Fig. 1 in Y12b). In Loop A, the standard LETKF is performed, defined as iteration zero, to compute the weights for the smoother. Loop B is used to perform the iterations after Loop A. In Loop B, the smoother is applied at the chosen lag time t_m ($t_{n-6} \le t_m < t_n$) to smooth the mean and ensemble anomalies using Eqs (6) and (7), respectively.

$$\overline{\mathbf{x}}_m^{a,i+1} = \mathbf{X}_m^{b,i}\overline{\mathbf{w}}_n^{a,i} + \overline{\mathbf{x}}_m^{b,i} \tag{6}$$

$$\mathbf{X}_m^{a,i+1} = \mathbf{X}_m^{b,i}\mathbf{W}_n^{a,i} \tag{7}$$

At the i^{th} iteration, the weights ($\overline{\mathbf{w}}_n^{a,i}$ and $\mathbf{W}_n^{a,i}$) obtained during the LETKF analysis computation at t_n are applied to the mean and the perturbations of the model ensemble at t_m ($\overline{\mathbf{x}}_m^{b,i}$ and $\mathbf{X}_m^{b,i}$). Eqs (6) and (7) start at $i = 0$, where $\overline{\mathbf{w}}_n^{a,0}$ and $\mathbf{W}_n^{a,0}$ are the weight coefficients from the standard LETKF (with the observation assimilated once) and $\overline{\mathbf{x}}_m^{b,0}$ and $\mathbf{X}_m^{b,0}$ are the mean and the perturbations of the forecast ensemble, which is initialized from the final analysis ensemble, as derived at the previous analysis time t_{n-6}. With Eqs (6) and (7), the updated ensemble at t_m includes the information at the later time t_n.

Forward integration of the ensemble states from t_m to t_n provides the new background ensemble ($\mathbf{x}_n^{b,i+1}$) for the next iteration. The LETKF computation is repeated in order to obtain the new analysis ensemble ($\mathbf{x}_n^{a,i+1}$) and weight coefficients ($\overline{\mathbf{w}}_n^{a,i+1}$ and $\mathbf{W}_n^{a,i+1}$). As proposed in KY10, this procedure could be repeated until some stopping criterion is fulfilled (Section 4.5), in order that the overfitting of observations is avoided; but in this study the RIP iteration was applied just once to explore its potential impact in a realistic assimilation setup under computational concerns.

3.2 The Weather and Research Forecasting Model and experimental settings

The Advanced Research WRF (ARW) model (Skamarock et al. 2005) used in this study has

been widely used to perform severe weather prediction and to study regional weather predictability (e.g., Zhang et al. 2006; Zhang et al. 2010; Torn et al. 2010; Miyoshi and Kunii 2011, Yang et al. 2013). The LETKF scheme is implemented with this model and the RIP method is then constructed based on the WRF-LETKF system. In this study, the model settings and the strategies for the use of the RIP method follow Y12b, who demonstrated the potential of the RIP method for typhoon assimilation and prediction with OSSE experiments. However, we modify the strategy further, in order to use RIP adaptively as an outer-loop in the LETKF framework.

The ARW (version 3.2) model domain is arranged to cover Taiwan and the area southeast of China and Japan, using a horizontal grid of 220×200 grid points with a horizontal spacing of 25 km. There are 28 vertical sigma layers with the top at sigma = 0.0065 (about 50 hPa). The physical parameterizations include: the Rapid Radiative Transfer Model (RRTM) based on Mlawer et al. (1997) for longwave radiation, the Dudhia (1989) shortwave radiation scheme, the Yonsei University (YSU) PBL scheme (Hong et al. 2006), the Kain–Fritsch scheme (Kain 2004) for cumulus parameterization, and the single-moment microphysics scheme by Lin et al. (1983). These settings are used in all the experiments.

The experiments focus on a period ranging from 0000 UTC 9 September 2008 to 0600 UTC 12 September 2008; the developing and intensifying stage of Typhoon Sinlaku. The observations for assimilation include upper air soundings from rawinsondes and aircraft reports, surface stations and dropsondes (Fig. 2).

The initial ensemble is cold-started at 0000 UTC 8 September 2008; 36 ensemble members are generated with initial conditions centered at the National Centers for Environmental Prediction (NCEP) Global Forecasting System (GFS) final analysis (FNL $1 \times 1°$ data), and the ensemble perturbations are drawn randomly from the 3D-Var background error covariance (Torn et al. 2006). The same procedure is used to perturb the NCEP FNL data every 6 hours until 0000 UTC 15 September; the tendencies are then computed at the boundaries according to these perturbed states in order to obtain the corresponding perturbed boundary conditions. The initial and boundary conditions of the 36 ensemble members are then used to initialize the assimilation experiments at 0000 UTC 8 September with an analysis interval of six hours. The RIP-related experiments start at 0000 UTC 9 September. We should note that RIP improves the use of observations, but during 8 September, it is not expected to accelerate the spin-up of the WRF-LETKF system yet,

because there are no observations (neither upper air soundings nor dropsondes) near the typhoon at that time.

As indicated by Y12b, the temporal de-correlation scale for using observations in such regional assimilations is about three hours, such that the window for applying the no-cost smoother is chosen to be three hours. Therefore, the smoother is applied at 0300, 0900, 1500, 2100 UTC with weights derived from the LETKF analysis performed at 0000, 0600, 1200 and 1800 UTC. With the adjusted (smoothed) ensemble states at 0300, 0900, 1500, 2100 UTC, a three-hour ensemble forecast is then carried out, followed by the second LETKF analysis to assimilate the observations once again. As a brief summary, the first RIP iteration performs the regular LETKF analysis with the 6-hr ensemble forecast as the background ensemble; the second RIP iteration re-assimilates the same observations with the 3-hr ensemble forecast evolved from the smoothed analysis ensemble (Fig. 1 from Y12b).

Using the observations more than once might violate the assumption that the observations and background information are independent. This is compensated by reducing the spread of the ensemble, as discussed in YKH12. Also, the issue of strong nonlinearity during the LETKF's spin-up could become more serious, which significantly limits the performance of EnKF.

4. Results

4.1 Error covariance

The goal of the RIP method is to improve simultaneously the structure of the background error covariance used for providing analysis corrections, and the accuracy of the mean state. With the improved ensemble members, the dynamical evolution can then be further improved, staying closer to the natural trajectory. In addition, the ensemble perturbations are expected to better present the uncertainties related to underlying dynamical instability associated with the development of the tropical cyclone. Therefore, we will first illustrate the structure of the error covariance during the spin-up and discuss the corresponding dynamical adjustments for the typhoon structure.

Figure 3 shows the error covariance between the zonal wind at the location (126°E, 19.5°N and near 750 hPa) and the zonal wind on the WRF eta level near 750 hPa. The error covariance is constructed with the background ensemble at 1200 UTC 9 September 2008, when Sinlaku is at the stage of tropical storm. The chosen location (marked with "●" in Fig.

3) is in the strong winds region of the typhoon (Fig. 4(d)) and the typhoon center is denoted by ×. From Fig. 3, both the LETKF and LETKF-RIP covariance structures show a negative covariance (indicated by red contours) south of the typhoon center. If a zonal wind observation is available at this chosen location and a westward wind correction is derived at this location, such a covariance pattern will introduce an eastward wind correction south of the typhoon center. Therefore, with this observation, an analysis increment characterized by cyclonic-circulation will be obtained and the typhoon circulation can be enhanced. From Fig. 3(b), it is evident that the negative pattern is more evident with RIP, suggesting a stronger cyclonic enhancement would be obtained. Also, the covariance structure in Fig. 3(a) is somewhat asymmetric and exhibits larger values away from the chosen point. As will be discussed later, the resulting corrections from Fig. 3(a) are not helpful for improving the dynamical structure of typhoon and might result in a less balanced circulation for the typhoon structure, which will affect the following track prediction.

Fig. 3(b) also suggests that at this time, error covariance with RIP is better "spun-up" to reflect the typhoon dynamics in nature. With the improved error covariance, the typhoon structure could be better represented. Figure 4(a and b) shows the near-surface wind speed, Fig. 4(c) is the difference between Fig. 4(a and b), and Fig. 4(d) is the observation from QuikSCAT near the same time. As shown in Fig. 4(a), the eyewall structure of the typhoon is better organized and the wind speed is stronger in the RIP analysis than shown in the standard LETKF analysis. Also, the strong vertical velocity (indicated by black contours) agrees with the strong winds in the RIP analysis, indicating a well-established eyewall for a rapidly intensifying typhoon. The difference shown in Fig. 4(c) indicates that stronger cyclonic circulation is obtained in the LETKF-RIP analysis, such that the typhoon circulation can be further enhanced. We note that such enhancement is not only shown in the horizontal, but extends towards the upper troposphere (figure not shown). In Fig. 4(a), strong winds located from the northeast to the south of the typhoon correspond well to the non-assimilated observed wind pattern (Fig. 4(d)). As with the results from the error covariance derived with the standard LETKF (Fig. 3a), strong winds in the LETKF analysis locate north of the typhoon center (Fig. 4(b)), exhibiting a less organized eyewall and an asymmetrical pattern towards the north side of the center. All these evidences suggest that the error covariance with RIP at this time could provide better analysis corrections for adjusting the typhoon circulation. The track forecast initialized with the LETKF-RIP analysis at 1200 UTC 9 September is also more accurate and the track error is 116 km with the 72-h forecast, compared to 173 km obtained from the forecast initialized from the standard LETKF analysis. Overall performance of track prediction will be further discussed

in sub-section 4.3.

4.2 Results from analysis

The performance of the LETKF and LETKF-RIP systems are first examined with the innovation statistics derived from the first two days (eight analysis cycles). Figure 5 shows the bias and root mean square (RMS) of the innovation (observation minus background) of the zonal and meridional winds. The amplitudes of the bias and RMS of the innovations are larger than the results shown in Miyoshi et al. (2011) or Jung et al. (2012), because the LETKF system is under spin-up and also because satellite data, such as the AMV winds, are not assimilated in this study. We also note that the "background" of the LETKF-RIP in Fig. 5 is the mean of the 6-h ensemble forecast, not from the 3-h ensemble forecast used for the second iteration. This is to ensure that the background states are independent from the observations that they are verified against. From Fig. 5(a), both the bias and RMS of the innovation of the zonal wind are reduced with the RIP method (in red lines), especially for levels below 700 hPa. The positive bias suggests that the westward component is too strong in the LETKF background, whereas that component is reduced in the LETKF-RIP background. This might also explain why the typhoon prediction initialized from the LETKF analyses has a stronger but less-realistic westward moving direction (e.g., Fig. 8(a)). The same improvement can also be identified in the lower troposphere in the bias of the innovation of the meridional wind. In addition, as the difference is most evident below 700hPa, this reflects the fact that during 9 and 10 September, the most effective adjustment derived from RIP is from the dropsondes employed by the C130 reconnaissance flight.

We also evaluate the analysis quality in terms of typhoon parameters, including: the position error, the 30-kts wind radii error, the central sea level pressure, and the maximum surface wind. On average, the LETKF and LETKF-RIP analyses, indicated by the blue and red solid lines, respectively in Fig. 6, show comparable ability in representing the typhoon location and intensity, both in terms of the central sea level pressure and the maximum surface wind. Nevertheless, the error of the 30-kts wind radii is significantly reduced when RIP is applied, and the associated adjustments can correct the too-broad typhoon circulation originally shown in the standard LETKF analysis. As discussed further in Section 4.3, the results from Fig. 6(b) suggest that the advantage of RIP is reflected in improving the environmental conditions for typhoon development, such that the size of the typhoon can be better represented in the LETKF-RIP analysis. The positive impact is particularly evident during the rapid intensification stage of the typhoon before 0000 UTC 11 September.

Regarding the typhoon intensity, we should note that with the resolution (25 km) used in the experiments, RIP has limited influence on representing the details of the inner core structure and therefore, has limited impact on modifying the typhoon intensity. Also, note that currently, the typhoon position is not assimilated; therefore, the RIP procedure would not be useful for correcting the typhoon position and might cause larger positional errors on 9 September, where there is no clear inner-core structure in the typhoon. Assimilating typhoon locations (Chen and Synder, 2007; Wu et al. 2010) might be helpful in constraining the typhoon position during early development.

4.3 Results from forecasts

In the following, we focus on the impact of the RIP method on the forecast performance during the first two days of the RIP experiment. As mentioned in Section 2, this period also corresponds to Sinlaku's rapid intensification from a tropical storm to a typhoon. Figure 7 shows the forecast performance in terms of typhoon parameters and the results are averaged from 0000 UTC 9 September to 1800 UTC 10 September (8 cases). In addition to the absolute error shown in Fig. 7(a), Fig. 7(b) presents the cross track error, which considers only the direction of the typhoon's movement and ignores the effects of its speed of movement. The typhoon track prediction is important for determining the landfall location and predicting the level of the accompanying precipitation. Results show that the track error of the forecasts initialized from the LETKF-RIP analysis is significantly reduced after the 36-h forecasts. This improvement reaches 80 km at the 3-day forecasts. In terms of the cross track error, such an improvement from using RIP can be identified even earlier, at the 30-h forecasts. The cross track error with the LETKF-RIP forecast remains at a level of 50 km or below; whereas that with the LETKF forecast increases linearly with time towards a level of 100 km after the 3-day forecast. Such improvement in the track prediction implies that the analysis corrections obtained from the RIP method have a positive impact on adjusting the environmental conditions of the typhoon, and further improve the movement of the typhoon through the steering flow, including its direction and speed of movement (Fig. 7(b and f)). With the improved environmental conditions and the better-established typhoon structure (e.g., Fig. 3(a)) for rapid intensification, the size of the typhoon is better represented with the LETKF forecast (Fig. 7(e)). Even though a small improvement has been derived for the maximum wind after the 36-hour forecast (Fig. 7(f)), we recognize that the LETKF-RIP forecasts over predict the central sea level pressure of the typhoon, resulting in a larger error in Fig. 7(d). This is particularly evident when the forecasts are initialized at 0600 and 1200 UTC 10 September, between the rapid intensification and mature stage.

Despite the too-low central sea level pressure, such results confirm that the dynamical adjustment for typhoon intensification is addressed through the RIP iterations.

Considering the track prediction initialized at 0600 UTC 9 September as an example, the typhoon in the LETKF forecast (the blue line in Fig. 8(a)) has a westward moving component that is too strong, because the subtropical high extends too far westward (e.g., the blue contour in Fig. 8(b)). In comparison, the subtropical high with the LETKF-RIP forecast agrees better with that in the FNL analysis[*]. During the forecast hours, the movement of the typhoon is dominated by the steering flow in the mid-high levels, as shown in Fig. 9. However, at these levels, the steering flow in the LETKF-RIP forecast (denoted by red wind bars) exhibits a northward direction, whereas a northwestward steering flow is shown in the LETKF forecast (denoted by blue wind bars). The outcome of the latter scenario, is that the typhoon turns westwards earlier towards central Taiwan. Also, the typhoon in the LETKF-RIP forecast has a stronger vertical development (Fig. 9(a)), supporting the stage of rapid intensification. In comparison, the typhoon in the LETKF forecast at mid-levels has a much broader structure. Furthermore, when defining the degree of the nonlinearity as the differences between the single forecast initialized from the analysis ensemble mean and the mean of the ensemble forecasts initialized at 0600 UTC 9 September, the results show that such a difference is much reduced in the LETKF-RIP forecasts during the first 48 hours. This suggests that the LETKF-RIP ensemble perturbations evolve more linearly with fewer outliers; whereas the nonlinear evolutions of the outliers of the LETKF ensemble dominate the ensemble forecasts, such that the mean of the ensemble forecast deviates quickly from the deterministic forecast initialized from the analysis ensemble mean. This also supports the findings of YKH12, in that applying the RIP method allows EnKF schemes better handling of the nonlinear dynamics and avoids the distribution of the ensemble being severely distorted by strong nonlinearity. Figure 10 shows the 25% and 75% quantiles of the ensemble track errors at different forecast hours. The 25% quantile of the ensemble track errors is comparable between the LETKF and LETKF-RIP forecasts at most of the forecast hours, but the 75% quantile of the LETKF ensemble track errors increases faster in time than that derived with the LETKF-RIP ensemble forecasts. At the 72-hr forecast, 15 members out of the 36 LETKF members have simulated a typhoon with a track error larger than 250 km, whereas there are only 8 members from the LETKF-RIP ensemble with the same criterion. This implies that one tail grows faster in the LETKF ensemble and

[*] The typhoon in the NCEP FNL analysis at this time is too weak and less organized, such that the track prediction is rather poor when initialized directly from the FNL analysis.

that the ensemble distribution is greatly distorted. As a result, the track error of the mean of the ensemble forecast is 205 and 113 km with the LETKF and LETKF-RIP forecast, respectively.

With the improved track prediction, the LETKF-RIP forecast allows better prediction of the landfall location, which positions the area of direct impact on Taiwan. Table 1 lists the errors of the landfall locations. It is clear that Sinlaku's landfall location is predicted more accurately by the LETKF-RIP forecasts, except when initialized at 0600 UTC 10 September. Even at an early assimilation time like 9 September, applying the RIP method with the same number of observations can better describe the potential of the typhoon hitting the northeastern part of Taiwan. We note that the issue regarding the forecast initialized at 0600 UTC 10 September is related to the overfitting of the same set of observations and this will be further discussed in Section 4.5.

4.4 Observation impact

Given that the track prediction is significantly improved during the LETKF's spin-up time, we can claim that the observations are used more effectively. To quantify this, we apply the ensemble-based method for estimating the observation impact proposed by Liu and Kalnay (2008). The formula has recently been updated in Kalnay et al. (2012):

$$\Delta e_p^2 = e_{t|0}^T e_{t|0} - e_{t|-6}^T e_{t|-6} = \frac{1}{K-1}(y - H(\overline{x}_{0|-6}^f))^T \mathbf{R}^{-1}\mathbf{Y}_0^a \mathbf{X}_{t|0}^{f^T} \mathbf{P}^T \mathbf{P}(e_{t|0} + e_{t|-6}) \quad . \tag{8}$$

In (8), Δe_p^2 measures the impact on the forecast at time t obtained by assimilating the observation at time 0. $e_{t|0} = \overline{\mathbf{x}}_{t|0}^f - \overline{\mathbf{x}}_t^a$ defines the forecast error at time t when initialized at time 0 and $\overline{\mathbf{x}}_t^a$, the analysis state at time t is used to approximate the true state. The same definition applies on $e_{t|-6} = \overline{\mathbf{x}}_{t|-6}^f - \overline{\mathbf{x}}_t^a$ for the forecast initialized at time -6. The operator $\mathbf{P}$ defines the forecast verification area. With this method for estimating observation impact, and also using the case of the 2008 typhoon Sinlaku, Kunii et al. (2012) demonstrate that the typhoon track prediction could be improved by removing the dropsonde observations with negative impact on the forecast. In this subsection, we focus on the impact obtained from the dropsonde data at 0600 UTC 9 September obtained by the C130 reconnaissance flight. This is also the first set of dropsonde data available for Sinlaku. During the WRF-LETKF's spin-up period, the information of the observations cannot be extracted effectively with a less-representative background error covariance. As shown in Fig. 8(a), the track prediction with the LETKF-RIP is significantly improved, especially at the longer forecast time. In the following, we will focus on the environmental conditions of the typhoon and the impact of

the observations is evaluated for the 2-day forecast and targeted for Sinlaku's environment (500 km away from typhoon eye). Forecast error is defined in relation to the kinetic energy. As for verification, the NCEP FNL analysis with a large number of observations assimilated is used to specify the true synoptic features representing the typhoon's environmental conditions, despite the fact that the TC structure is not represented well owing to the model resolution.

Figure 11 shows the horizontal map of the impact of the observations. Negative values indicate that positive impact is derived from observations. In other words, the 2-day forecast errors outside the typhoon could be reduced by assimilating the dropsondes. Figure 9(b) shows that with the standard LETKF, most of the dropsonde data could provide positive impact. With RIP, the positive impact is largely enhanced. Wu et al. (2012a) also conclude that the dropsondes could provide a positive impact on the environmental conditions of the typhoon with the global assimilation system. Figure 12 compares the averaged impact per dropsonde on the standard LETKF and LETKF-RIP forecasts. Results suggest that the improvement gained with RIP is mainly located below 700 hPa. At 600 hPa, the observation impact from LETKF-RIP is worse than that derived from the standard LETKF. However, such a difference is not statistically significant because there are only eight observations available near 600 hPa, which is much fewer than the number of observations below 700 hPa. We also notice that most of the dropsonde data east of the eye does not pass the quality check procedure, owing to the very strong meridional wind near the typhoon eyewall. Although these data might represent the strong intensity of the typhoon at that time, assimilating them might not be helpful for the "synoptic-scale" pattern.

Overall, the results from Figs 11 and 12 suggest that the effectiveness of the dropsonde data could be greatly improved by the RIP method, which aims to extract most of the observation information by simultaneously improving the ensemble mean and error covariance.

4.5 RIP with a stopping criterion

KY10 showed that if RIP is always used at each analysis cycle with the same iteration number, the analysis accuracy actually degrades because the ensemble has overfitted observations. With the WRF model, Y12b show that the advantage from using the LETKF-RIP saturated after two-day assimilation (8 analysis cycles). KY10 and YHK12 suggest that a stopping criterion, based on the statistics of the innovation vector, should be applied to avoid such overfitting. In the following, we test whether a stopping criterion could be applied to turn RIP off or on automatically when needed, rather than assuming a fixed spin-

up period. If the error statistics beyond the spin-up period change abruptly due to strong nonlinear evolution of the underlying flow, it might be desirable to switch RIP on again. For example, the direction of movement of Sinlaku switches from northwards to northwestwards after 1200 UTC 11 September and to northeastwards after 0000 UTC 15 September. These features indicate that there are significant modifications in the environmental conditions of the typhoon. In addition, on 11 September, the typhoon intensity starts to decay; further indication of dynamic changes of state in the typhoon. Therefore, we would like to investigate whether RIP should be switched on again to "spin-up" further the ensemble-based error covariance.

Figure 13 is the track prediction initialized at 0600 UTC 10 September based on the standard LETKF analysis, and analyses from the two iterations of LETKF-RIP. The analysis from the first iteration (Loop A) of RIP is regarded as a temporary product and the one from the second RIP iteration (Loop B) is the final LETKF-RIP analysis. At this time, the typhoon track (blue line) has already been well predicted in the LETKF forecast. With RIP, the track prediction initialized from the LETKF-RIP analysis actually degrades (red solid line), compared with the one initialized from the analysis derived at the first iteration (red dashed line). This implies that the RIP iteration is not necessary at this time. Actually, there is sufficient information near Sinlaku because dropsondes are available at both 0000 UTC and 0600 UTC 10 September (Fig. 2(d and e)).

In order to automatically stop RIP, ε in (9) is used to determine whether we are able to extract more information from the same set of observations.

$$\varepsilon = \frac{RMS\_Innov_i - RMS\_Innov_{i+1}}{RMS\_Innov_i} \times 100\% \tag{9}$$

In (9), *i* is the index of the iteration number and RMS_Innov_i is the variance of the innovation normalized by the observation error variance $(y - H(\overline{x}_b^i))^T \mathbf{R}^{-1} (y - H(\overline{x}_b^i))$. We note that in this study only the wind observations are used for computing (9). The RIP iteration will only continue when $\varepsilon > 15\%$ and in the following, the LETKF-RIP experiment with this stopping threshold applied is referred to as LETKF-RIP-TRS.

Figure 12 shows the time series of ε. The results suggest that RIP is particularly desirable for the first day for the purpose of spinning up the LETKF system, and should be reactivated at 0000 UTC 10 September and at 1800 UTC 11 September. According to Fig. 14, RIP is not required at 0600 UTC 10 September, as suggested in Fig. 11. As shown in Fig. 13(a), the forecast initialized from the LETKF-RIP-TRS analysis (with the stopping

criterion and denoted by the red line) could avoid the negative impact from overfitting observations. We note that this initial time (0600 UTC 10 September) is also the only time that the LETKF-RIP forecast has a larger landfall location error than the standard LETKF forecast (Table 1), but now the landfall location is very well predicted in the LETKF-RIP-TRS forecast.

When initialized at 1800 UTC 11 September, the typhoon in the LETKF forecast has a sharply southward-deflected track (the blue dashed line in Fig. 15(b)). As the typhoon approaches Taiwan, the northerly to the west of the typhoon becomes stronger. Such track deflection is related to an enhanced channel wind effect, which results from an intense interaction between the typhoon and the topography (Lin et al. 1999; 2005; Huang et al. 2012). In the LETKF forecast, the typhoon has a stronger westward moving component, such that the typhoon turns more westward than in the LETKF-RIP-TRS forecast. By impinging on the central part of Taiwan, this results in a stronger interaction between the typhoon in the LETKF forecast and the topography of Taiwan. Therefore, the channeling effect is more evident and thus, the northerly to the west of typhoon is more enhanced in the LETKF forecast, even though the forecasts are not derived at a high resolution, which is suggested as a requirement in simulating the southward deflection of the typhoon (Huang et al. 2012). When initialized from the LETKF-RIP-TRS analysis, the track prediction is improved, as the LETKF-RIP forecast has already demonstrated, and the unrealistic southward track deflection is again corrected as the typhoon approaches Taiwan. This confirms that the dynamical adjustment introduced by the RIP iteration is useful for improving the environmental conditions for typhoon movement prior the landfall. When comparing the maximum wind speed of the typhoon in the analyses from both iterations in LETKF-RIP-TRS, the result shows that the maximum wind speed is significantly reduced in the analysis from the second iteration (57.4 m s^{-1} vs. 61.5 m s^{-1}). A similar change is also found in the analyses during the LETKF-RIP iterations at this time, which suggests that the RIP iteration is needed again at this time in order to "catch up" the decaying stage (spin-down) of the typhoon. Although there are no dropsonde data available at this time, the main impact from RIP is from one rawindsonde at (124.17°E and 24.33°N).

When defining the degree of nonlinearity as the difference between the forecast initialized from the ensemble mean state and the mean of the ensemble forecast, such a difference derived from the LETKF forecast is more than twice that derived from the LETKF-RIP forecast during the early forecast hours prior to landfall. Figure 16 shows the 25%, 50% and 75% quantiles of the ensemble track errors from the LETKF, LETKF-RIP and LETKF-RIP-TRS ensemble forecasts. Fig. 16(a) shows that the median of the LETKF

ensemble tracks inclines to the 75% quantile, whereas the median locates more evenly between the 25% and 75% quantiles in both the LETKF-RIP and LETKF-RIP-TRS ensemble tracks. Therefore, Fig. 16(c) suggests that it is indeed helpful to adjust the nonlinearity of the ensemble distribution after switching on RIP, even after the LETKF's spin-up.

On average, the improvement from applying a stopping criterion is most significant in terms of the cross track error related to the direction of movement. As shown in Fig. 17, by removing the negative impact from overfitting, the cross track error of the LETKF-RIP-TRS forecast during the first 36-hour forecast is improved. The results suggest that an automatic criterion for using RIP could further enhance the performance of the RIP method, such that overfitting is avoided. Most importantly, the RIP method could serve as a generalized outer-loop procedure, as suggested by YKH12, not only to accelerate the EnKF's spin-up but also to improve adaptively the nonlinear evolution of the ensemble during strong nonlinear dynamics.

5. Summary and Conclusions

In this study, the RIP method proposed by Kalnay and Yang (2010) is implemented in the WRF-LETKF system and applied to the real case of typhoon Sinlaku in 2008. The goal of this study is to explore the feasibility of the RIP method in improving the performance of LETKF during the spin-up (or spin-down) periods and to serve as an outer-loop iteration to deal with strong nonlinear dynamics. For the purpose of typhoon assimilation, the former cases relate to typhoons in developing stages and the latter relate to typhoons undergoing rapid change.

The results suggest that during the LETKF spin-up period, the ensemble-based error covariance could be improved through the RIP iterations and better corresponds to the cyclonic circulation of the typhoon. With such covariance structure, the observations could be used effectively and the circulation of the typhoon in the LETKF-RIP analysis is enhanced and more organized than that in the standard LETKF analysis. Compared with the unassimilated QuikSCAT surface winds, the LETKF-RIP analysis represents successfully the strong wind region when Sinlaku is undergoing rapid intensification from the tropical storm stage.

Overall, the results show that the track error beyond the 36-h forecast, initialized from the LETKF-RIP analysis, is reduced in comparison with the standard LETKF forecast, and that the improvement in the cross track error is even more evident. This implies that the RIP method provides useful dynamical adjustment for the environmental conditions of the

typhoon. When initializing from the LETKF-RIP analysis on 9 September, the track prediction can be significantly improved from that initialized from the standard LETKF analysis, and such an advantage is attributed to the better representation of the environmental conditions of the typhoon, such as the eastward retreat of the subtropical high at a later time. With an ensemble-based tool (Kalnay et al. 2012) for estimating the observation impact on reducing forecast errors, we also found that the first available dropsondes at 0600 UTC 9 September could be used more efficiently in reducing the forecast errors of the environmental conditions of the typhoon. Such impact is particularly identifiable below 700 hPa in the environmental conditions of the typhoon.

Instead of using RIP all the times, we follow YKH12 to further use RIP as an outer-loop. A stopping criterion associated with the innovation statistics is defined to use the RIP method automatically and to avoid the overfitting of the observations. Results suggest that the RIP should be used only if it is needed. When there are sufficient observations covering the typhoon, no further advantage can be gained from the RIP iteration, in addition to the standard LETKF procedure. However, when the typhoon undergoes rapid change, the RIP method should be re-activated again, in order to adjust its ensemble evolution. Results using the LETKF-RIP analysis at 1800 UTC 11 September show that the background ensemble carries the tendency of strong intensification of the typhoon, whereas the observation shows a feature of decaying. By reactivating the RIP method, it allows the reduction of the typhoon intensity in the analysis ensemble and the unrealistic track deflection related to the channel wind effect can be corrected. By switching RIP on, the Gaussianity of the ensemble distribution is better maintained. In comparison, the LETKF ensemble is dominated by outliers.

Results from this study confirm the feasibility of the RIP method and the conclusions from Yang et al. (2012b) with OSSE experiments. However, we should note that the results also show limited influence on representing typhoon intensity with the RIP method, and this should be related to the model resolution used in this study. The application of the RIP method will be investigated further with high-resolution grids and a nested domain setup. Also, limited by the model behavior, the problem of the speed of movement of the typhoon is still evident with the LETKF-RIP analyses. Observations, which are helpful for improving the geopotential fields, could be included and further emphasized through the RIP method.

Acknowledgement

The authors are grateful to Profs. Chu-Chieh Wu and I-I Lin from the National Taiwan University and Prof. Hunt from the University of Maryland for valuable discussions and

suggestions. The authors are also very grateful for computational resources from Academic Sinaca. S-C Yang and K-J Lin are sponsored by the National Science Council grant of Taiwan NSC-101-2111-M-008-020. T. Miyoshi is sponsored by the Office of Naval Research (ONR) grant N000141010149 under the National Oceanographic Partnership Program (NOPP).

References:

Aberson, S. D., 2003: Targeted observations to improve operational tropical cyclone track forecast guidance. *Mon. Wea. Rev.*, **131**, 1613–1628.

----------, 2011: The impact of dropwindsonde data from the THORPEX– Pacific Area Regional Campaign and the NOAA Hurricane Field Program on tropical cyclone forecasts in the Global Forecasting System. *Mon. Wea. Rev*., **139**, 2689–2703.

Caya, C., J. Sun, C. Snyder, 2005: A comparison between the 4D-VAR and the Ensemble Kalman Filter techniques for radar data assimilation. *Mon. Wea. Rev.* **133**: 3081–3094.

Chen, Y., and C. Snyder, 2007: Assimilating vortex position with an ensemble Kalman filter. *Mon. Wea. Rev.*, **135**, 1828–1845.

Chou, K.-H., C.-C.Wu et al., 2011: The Impact of Dropwindsonde Observation on Typhoon Track Forecasts in DOTSTSR and T-PARC. *Mon. Wea. Rev.,* **139,** 1728–1743.

Dirren, S., R.D. Torn, and G.J. Hakim, 2007: A data assimilation case study using a limited-area ensemble Kalman filter. *Mon. Wea. Rev*., **135**, 1455–1473.

Dudhia, J., 1989: Numerical study of convection observed during the Winter Monsoon Experiment using a mesoscale two-dimensional model. *J. Atmos. Sci*., **46**, 3077–3107.

Elsberry, R.L., and P.A. Harr, 2008: Tropical cyclone structure (TCS08) field experiment science basis, observational platforms, and strategy. Asia-Pac. *J. Atmos. Sci.*, **44**, 209–231.

Evensen, G., 2003: The ensemble Kalman filter: Theoretical formulation and practical implementation. *Ocean Dyn.*, **53**, 343–367.

Harnisch, F., and M. Weissmann, 2010: Sensitivity of typhoon forecasts to different subsets of targeted dropsonde observations. *Mon. Wea. Rev*., **138**, 2664–2680.

Hong, S.-Y., Y. Noh, and J. Dudhia, 2006: A new vertical diffusion package with an explicit treatment of entrainment processes. *Mon. Wea. Rev*., **134**, 2318–2341.

Huang, Y.-H., M.T. Montgomery, and C.-C. Wu, 2012: Concentric eyewall formation in Typhoon Sinlaku (2008). Part II: Axisymmetric dynamical processes. J. Atmos. Sci., **69**, 662–674.

Huang, Y-H, C.-C. Wu, and Y. Wang, 2012: The influence of island topography on typhoon track deflection. *Mon. Wea. Rev*., **139**, 1708-1727.

Hunt, E. J. Kostelich, and I. Szunyogh, 2007: Efficient data assimilation for spatiotemporal chaos：A local ensemble transform Kalman filter. *Physica D*, **230**, 112-126.

Jung, B. J., H.-M. Kim, F. Zhang, and C.-C. Wu, 2012: Effect of targeted dropsondes

observations and best track data on the track forecasts of Typhoon Sinlaku (2008) using an ensemble Kalman filter. TellusA, 64, 14984, DOI: 10.3402/tellusa.v64i0.14984.

Kain, J. S., 2004: The Kain–Fritsch convective parameterization: An update. *J. Appl. Meteor.*, **43**, 170–181.

Kalnay, E., H. Li, T. Miyoshi, S.-C. Yang and J. Ballabrera-Poy, 2007b: Response to the Discussion on "4D-Var or EnKF?" by Nils Gustaffson. *Tellus A*, **59**, 778-780.

——, S.-C. Yang, 2010: Accelerating the spin-up of Ensemble Kalman Filter. *Q.J.R. Meteorol. Soc*., **136**: 1644-1651.

——, Y. Ota, T. Miyoshi, J. Liu, 2012: A Simpler Formulation of Forecast Sensitivity to Observations: Application to Ensemble Kalman Filters. *Tellus A*, **64**, 18462.

Kunii, M., T. Miyoshi, and E. Kalnay, 2012: Estimating impact of real observations in regional numerical weather prediction using an ensemble Kalman filter. *Mon. Wea. Rev.*, **140**, 1975-1987.

Lander, M. A., 1996: Specific tropical cyclone track types and unusual tropical cyclone motions associated with a reverse oriented monsoon trough in the western North Pacific. *Wea. Forecasting*, **11**, 170–186.

Lawson, W. G. and J. A. Hansen, 2004: Implications of stochastic and deterministic filters as ensemble-based data assimilation methods in varying regimes of error growth. *Mon. Wea. Rev*, **132,** 1966–1981.

Lin, I.-I., C. C. Wu, K. A. Emanuel, I. H. Lee, C. R. Wu, and I. F. Pun, 2005: The interaction of Supertyphoon Maemi (2003) with a warm ocean eddy. Mon. Wea. Rev., 133, 2635–2649.

Lin, Y.-L., R. D. Farley, and H. D. Orville, 1983: Bulk parameterization of the snow field in a cloud model. *J. Climate Appl. Meteor*., **22**, 1065–1092.

Lin, Y.-L., J. Han, D. W. Hamilton, and C.-Y. Huang, 1999: Orographic influence on a drifting cyclone. *J. Atmos. Sci*., **56**, 534–562.

Liu, J., and E. Kalnay, 2008: Estimating observation impact without adjoint model in an ensemble Kalman filter. *Quart. J. Roy. Meteor. Soc.*, **134**, 1327–1335.

Miyoshi, T., 2011: The Gaussian approach to adaptive covariance inflation and its implementation with the local ensemble transform Kalman filter. *Mon. Wea. Rev.*, **139**, 1519–1535.

——, and M. Kunii, 2011: The local ensemble transform Kalman filter with the Weather Research and Forecasting model: Experiments with real observations. *Pure Appl. Geophys.*, **169**, 321-333.

Mlawer, E. J., S. J. Taubman, P. D. Brown, M. J. Iacono, and S. A. Clough, 1997: Radiative transfer for inhomogeneous atmosphere: RRTM, a validated correlated-k model for the long-wave. *J. Geophys. Res*., **102** (D14), 16 663–16 682.

Skamarock, W. C., J. B. Klemp, J. Dudhia, D. O. Gill, D. M. Barker, W. Wang, and J. G. Powers, 2005: A description of the Advanced Research WRF version 2. NCAR Tech. Note TN-468_STR, 88 pp.

Torn, R. D., G. J. Hakim, and C. Snyder, 2006: Boundary conditions for limited-area ensemble Kalman filters. *Mon. Wea. Rev.*, **134,** 2490–2502.

——, 2010: Performance of a mesoscale ensemble Kalman filter (EnKF) during the NOAA high-resolution hurricane test. *Mon. Wea. Rev*., **138**, 4375–4392.

Weissmann, M., and Co-authors, 2011: The influence of assimilating dropsonde data on typhoon track and mid-latitude forecasts. *Mon. Wea. Rev.*, **139**, 908–920.

Wu, C.-C.*, T.-S. Huang, and K.-H. Chou, 2004: Potential vorticity diagnosis of the key factors affecting the motion of Typhoon Sinlaku (2002). *Mon. Wea. Rev*., 132, 2084-2093.

_____, P.-H. Lin, S. Aberson, T.-C. Yeh, W.-P. Huang, and co-authors, 2005: Dropsonde observation for typhoon surveillance near the Taiwan Region (DOTSTART): an overview. *Bull. Am. Meteorol. Soc*., **86**, 787-790.

_____, K.-H. Chou, P.-H. Lin, S. D. Aberson, M. S. Peng, and T. Nakazawa, 2007: The impact of dropwindsonde data on typhoon track forecasts in DOTSTAR. *Wea. Forecasting*, **22**, 1157–1176.

——, G.-Y. Lien, J.-H. Chen, and F. Zhang, 2010: Assimilation of tropical cyclone track and structure based on the ensemble Kalman filter (EnKF). *J. Atmos. Sci.*, **67**, 3806–3822.

——, S.-G. Chen, C.-C. Yang, and P.-H. Lin, 2012a: Potential vorticity diagnosis of the factors affecting the track of Typhoon Sinlaku (2008) and the impact from dropwindsonde data during T-PARC. *Mon. Wea. Rev*., **140**, 2670-2688.

——, Y.-H. Huang, G.-Y. Lien, 2012b: Concentric Eyewall Formation in Typhoon Sinlaku (2008). Part I: Assimilation of T-PARC Data Based on the Ensemble Kalman Filter (EnKF). *Mon. Wea*. *Rev*., **140**, 506-527.

Wang, S., M. Xue, A. D. Schenkman, J. Min, and M. Xue, 2013: An Iterative Ensemble Square Root Filter and Tests with Simulated Radar Data for Storm Scale Data Assimilation, *Q. J. R. Meteorol. Soc*. DOI: 10.1002/qj.2077

Yang, S.-C., M. Corazza, A. Carrassi, E. Kalnay, T. Miyoshi, 2009: Comparison of ensemble-based and variational-based data assimilation schemes in a quasi-

geostrophic model. *Mon. Wea. Rev.* **137**: 639–709.

——, ——, B. Hunt, 2012a: Handling Nonlinearity in an Ensemble Kalman Filter: Experiments with the Three-Variable Lorenz Model. *Mon. Wea. Rev.*, **140**, 2628–2646.

——, E. Kalnay, and T. Miyoshi, 2012b: Accelerating the EnKF Spin-up for Typhoon Assimilation and Prediction, *Wea. Forecasting*, **27**, 878–897.

——, S.-Y. Chen, S.-H. Chen, C.-Y. Huang and C.-S. Chen, 2013: Evaluating the impact of the COSMIC-RO bending angle data on predicting the heavy precipitation episode on 16 June 2008 during SoWMEX-IOP8. *Mon. Wea. Rev*., under revision.

Zhang, F., Z. Meng, and A. Aksoy, 2006: Test of an ensemble Kalman filter for mesoscale and regional-scale data assimilation. Part I: Perfect model experiments. *Mon. Wea. Rev.*, **134**, 722-736.

——, Y. Weng, Y.-H. Kuo, J. S. Whitaker, B. Xie: 2010: Predicting typhoon Morakot's catastrophic rainfall with a convection-permitting mesoscale ensemble system. *Wea. Forecasting*, **25**, 1816-1825.

List of Tables

List of Figures

typhoon in the LETKF (LETKF-RIP) forecast in the vertical, and those at the bottom are the deep layer mean wind.

Figure 10 The 25% and 75% quantiles of the ensemble track errors from the LETKF and LETKF-RIP ensemble forecasts initialized at 0600 UTC 9 September.

Figure 11 Forecast sensitivity verified at 0600 UTC 11 September with respect to the dropsondes at 0600 UTC 9 September with results of the (a) LETKF-RIP and (b) LETKF analyses and forecasts.

Figure 12 Vertical distribution of the observation impact per dropsonde. The red line denotes the results obtained with the LETKF-RIP experiment and the blue line denotes the LETKF results.

Figure 13 Typhoon track prediction initialized at 0600 UTC 10 September with the LETKF (blue) and LETKF-RIP analysis from Loop A (red dashed line, also the first iteration) and from Loop B (red solid line, also the second iteration). Green dots are the locations of the dropsondes.

Figure 14 Time series of the ratio ε. The grey line indicates the stopping criterion (15%) to automatically switch the RIP iterations on (ε > 15%) or off.

Figure 15 (a) Typhoon track prediction initialized at 0600 UTC 10 September 10 with the LETKF (blue dashed line), LETKF-RIP analysis (blue solid line), and LETKF-RIP-THS analysis (red solid line). (b) Same as (a) except the initial time is 1800 UTC 11 September.

Figure 16 The 25%, 50% and 75% quantiles of the ensemble track errors from: (a) the LETKF, (b) LETKF-RIP and (c) LETKF-RIP-TRS ensemble forecasts initialized at 1800 UTC 11 September.

Figure 17 Mean cross track error from the LETKF and LETKF-RIP forecasts at different forecast hours averaged from the cases initialized at 0000 UTC 9 September to 0600 UTC 12 September with a 6-h interval.

Table 1 Errors of the typhoon landfall (km) from the forecasts initialized during 9-10 September 2008

time	LETKF	LETKF-RIP
0600 UTC 09	130	87
1200 UTC 09	87	43
1800 UTC 09	77	21
0000 UTC 09	13	11
0600 UTC 10	47	87
1200 UTC 10	47	32
1800 UTC 10	60	0

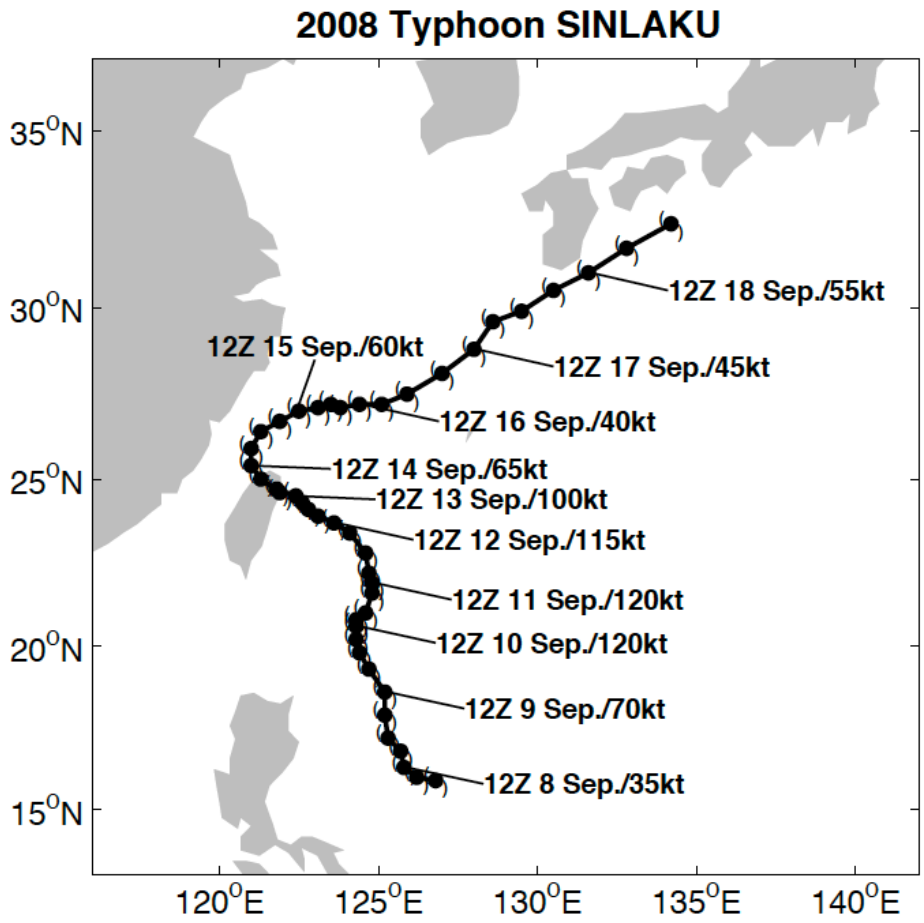

Figure 1 JTWC best track and intensity of typhoon Sinlaku 2008. Data are plotted every 6-h.

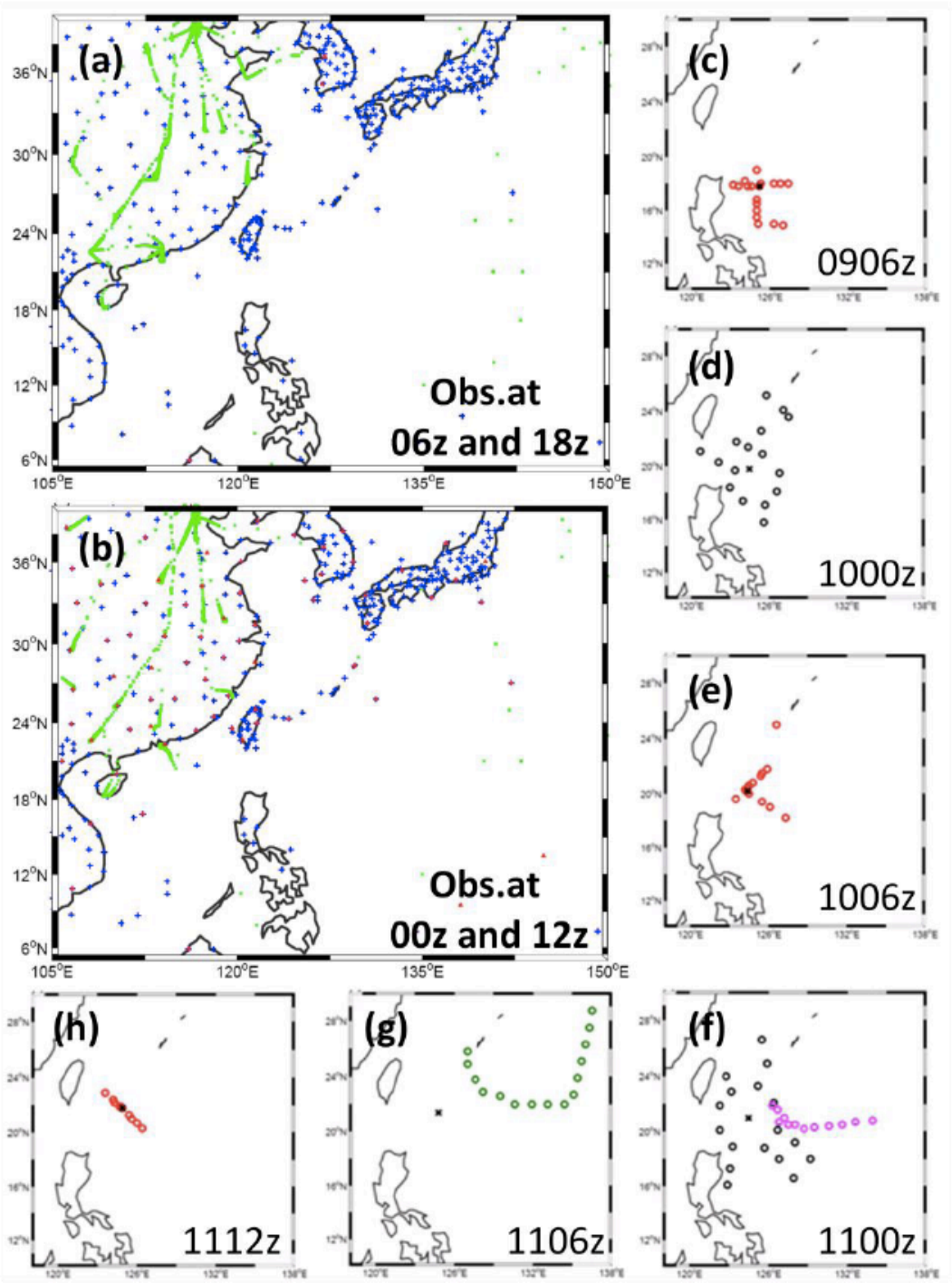

Figure 2 Observation distributions at different times: (a) typical distributions for upper air soundings and surface stations at 0600 UTC and 1800 UTC; (b) the same as (a), but for 0000 UTC and 1200 UTC; (c)-(h) are dropsondes available at different analysis times. Dropsondes from the USAF C130, DLR Falcon, NRL P-3 and ROTSTAR ASTRA flights are indicated by red, green, purple, and black open circles.

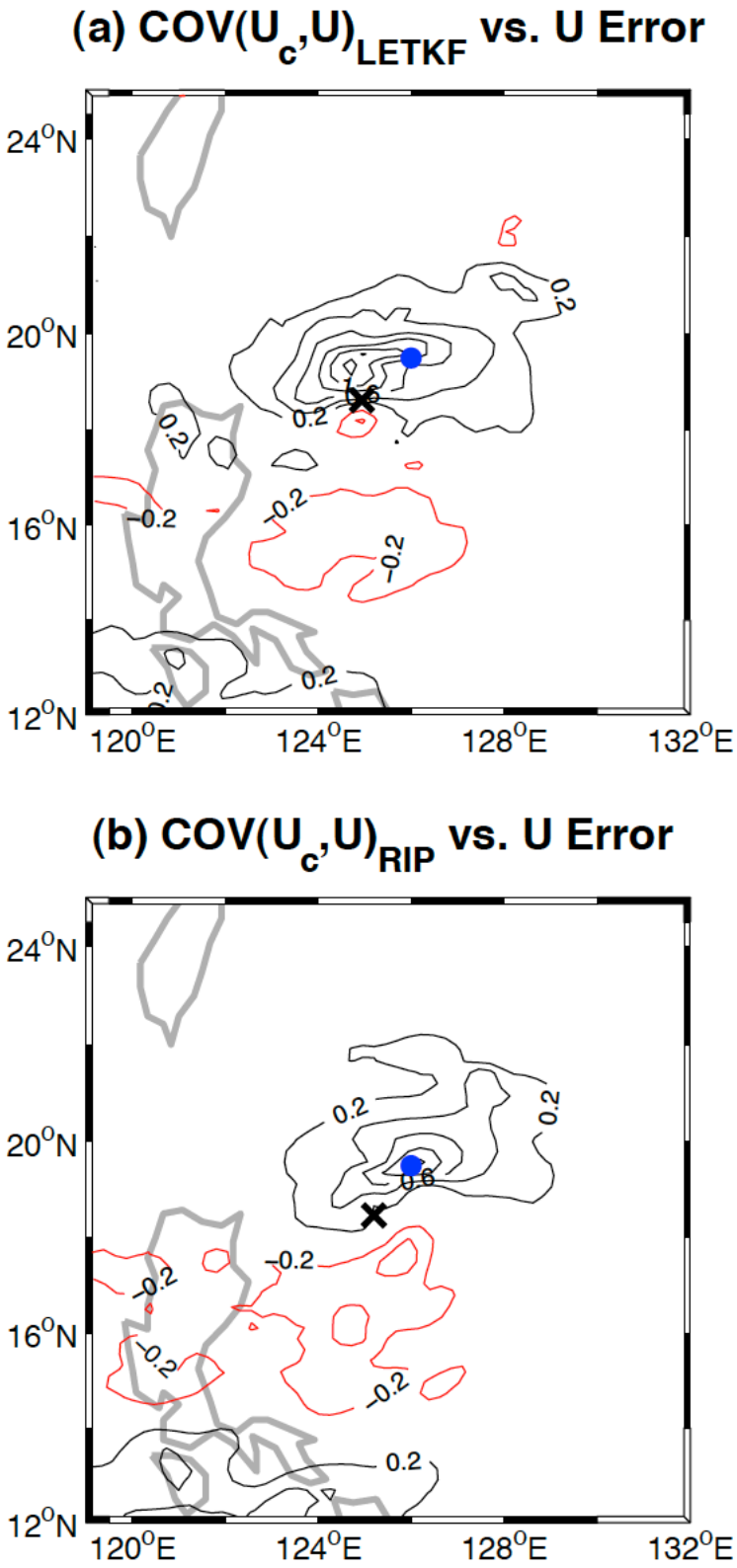

Figure 3 Error covariance structure (contours) between the zonal wind speed at the location (126°E, 19.5°N and about 750 hPa) marked with a '●' and the zonal wind speed on the WRF eta level near 750 hPa from the LETKF-RIP background ensemble at the first iteration at 1200 UTC 9 September. (b) The same as in (a), except the error covariance is derived from the LETKF background. Black contours denote the positive values and red contours the negative values. The cross marks (×) denote the center of the typhoon.

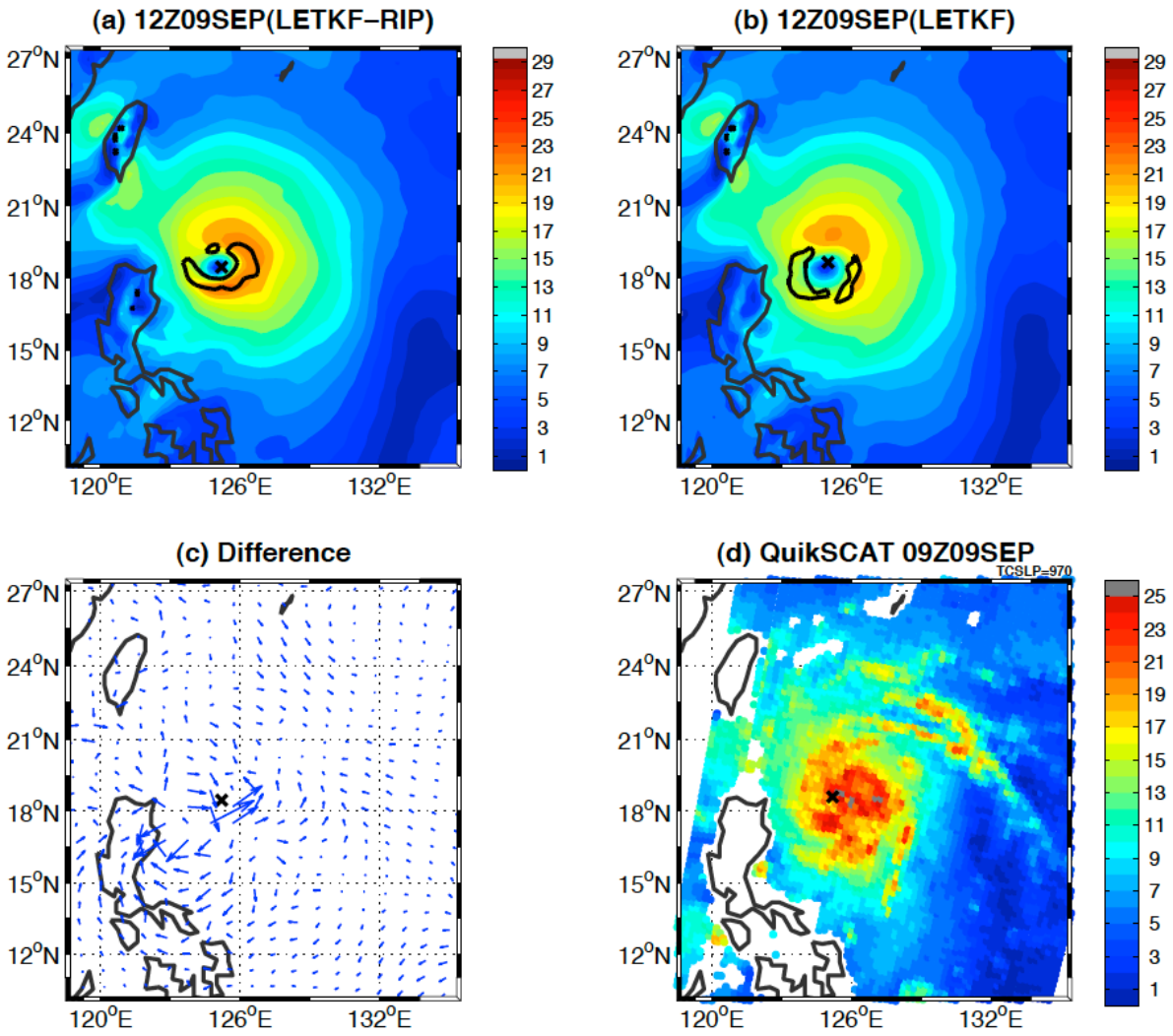

Figure 4 (a) Near-surface wind speed of the LETKF-RIP analysis at 1200 UTC 9 September, (b) the same as (a), except from the LETKF analysis, (c) the difference of the near-surface wind speed between the LETKF-RIP and LETKF analysis, and (d) wind speed from the QuikSCAT at 1200 UTC 9 September. The cross marks (×) denote the center of the typhoon.

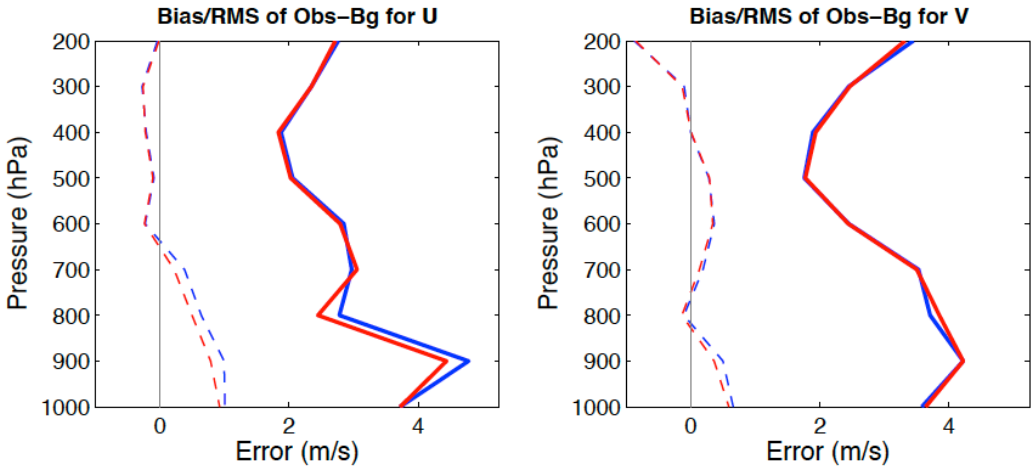

Figure 5 (a) bias (dashed lines) and RMS (solid lines) of the innovation vectors for the zonal velocity, (b) the same as (a) except with meridional velocity. Results with the LETKF and LETKF-RIP background are denoted in blue and red colors, respectively.

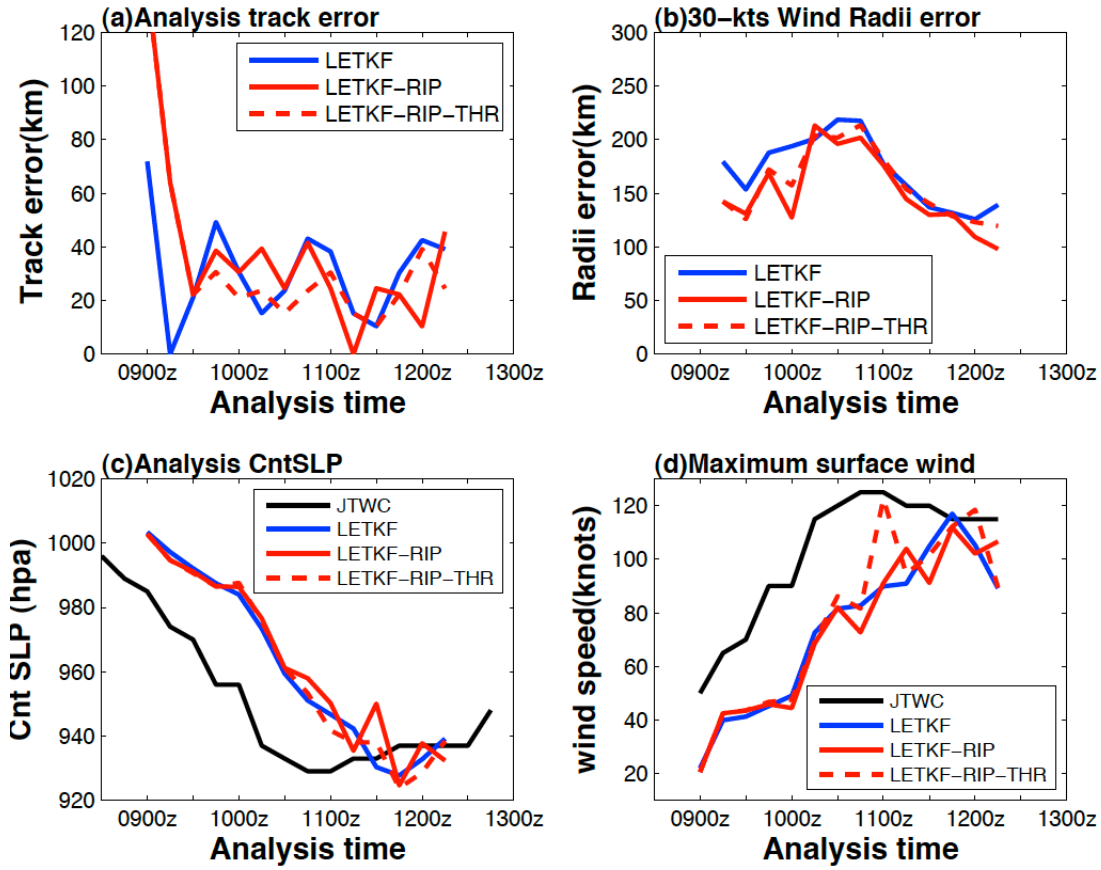

Figure 6 Analysis errors of typhoon-related parameters: (a) track, (b) 30-kts wind radii, (c) sea-level pressure at typhoon center, and (d) maximum surface wind.

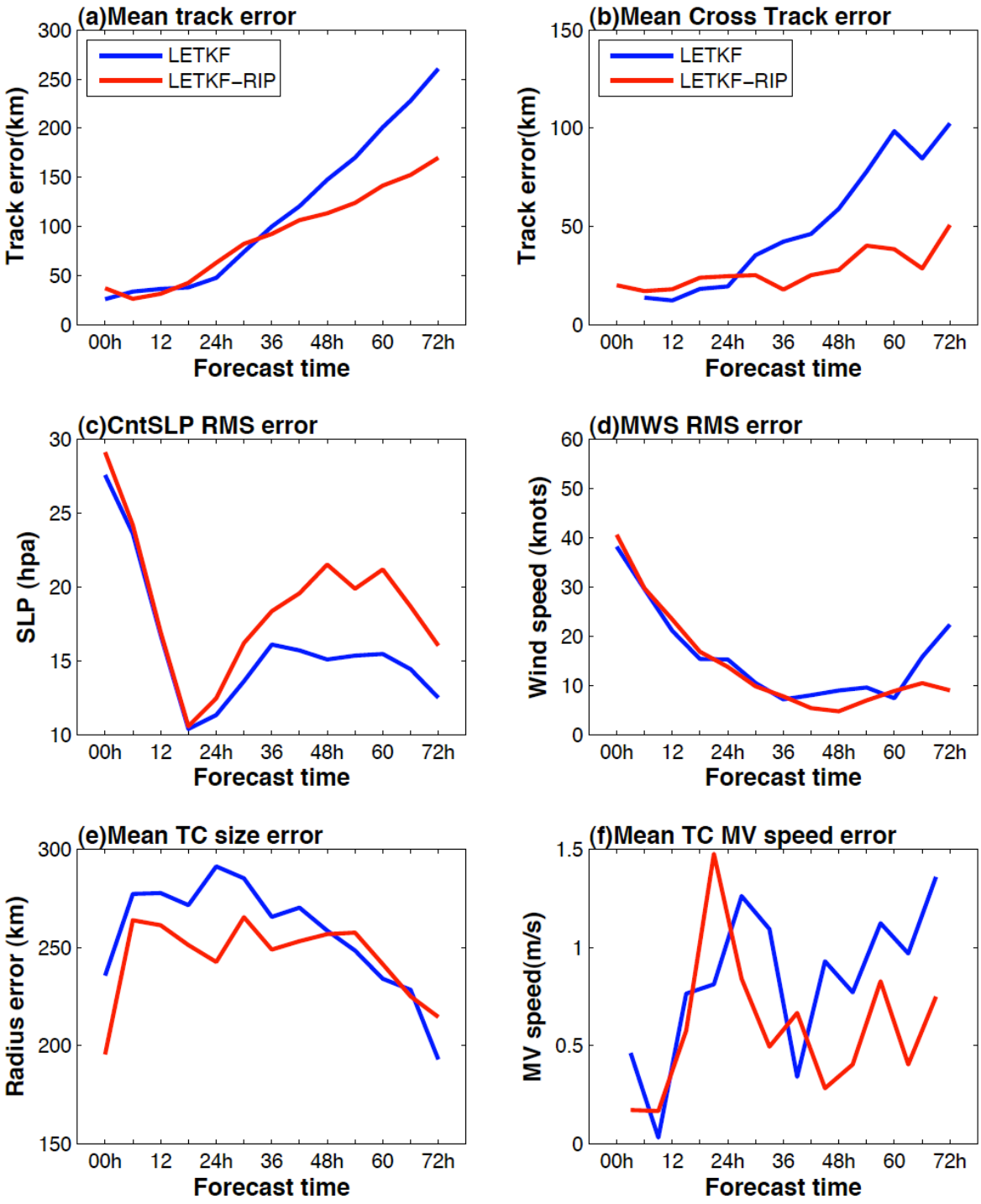

Figure 7 Mean errors associated with typhoon parameters from the LETKF and LETKF-RIP forecasts at different forecast hours: (a) absolute track (b) cross track error, (c) sea-level pressure at typhoon center, (d) maximum wind speed, (d) size of the typhoon and (f) is the mean translation speed of the typhoon.

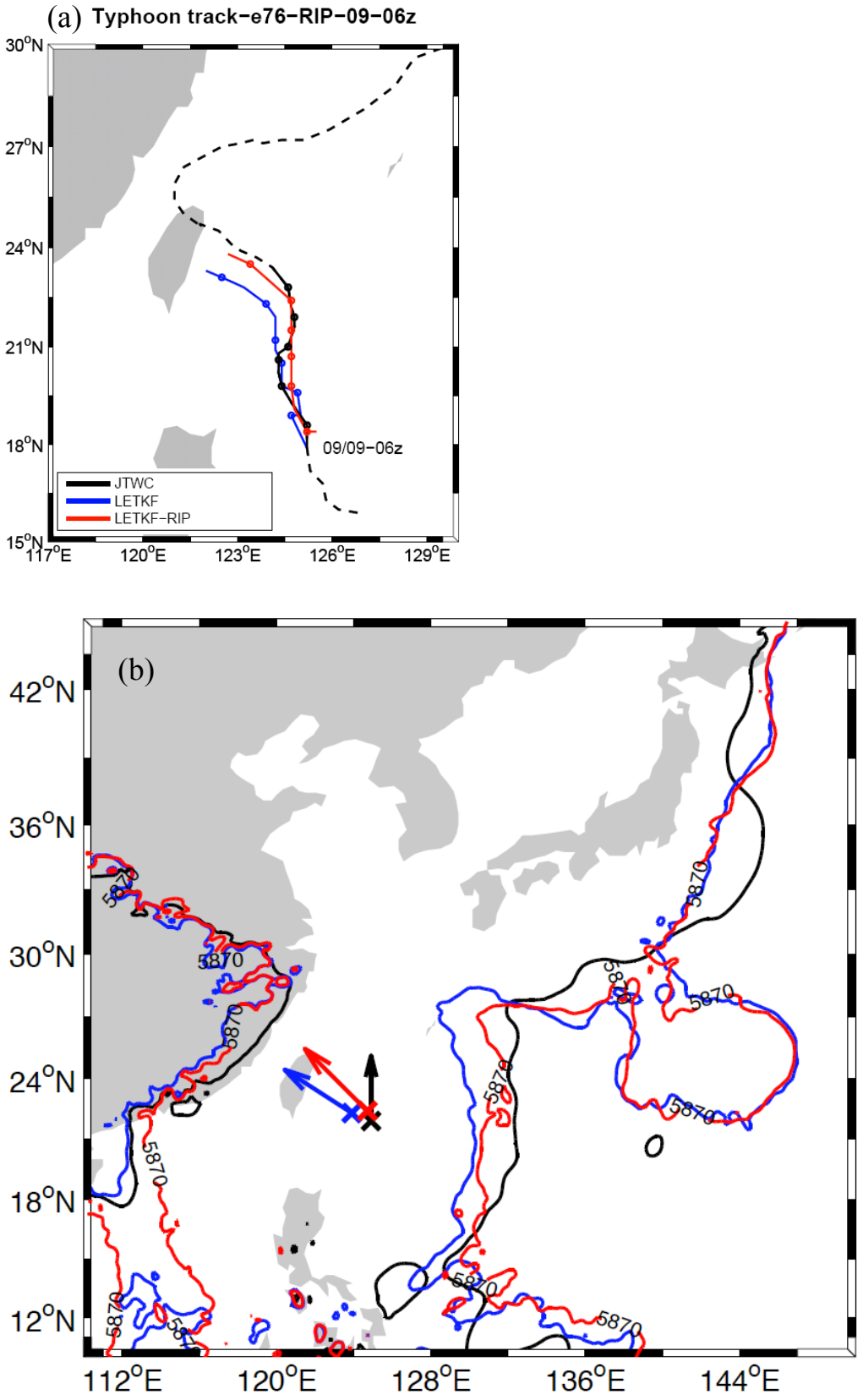

Figure 8 (a) Typhoon track prediction initialized at 0600 UTC 9 September with the LETKF (blue) and LETKF-RIP analysis (red line). (b) The 5880 isolines of the 500 hPa geopotential height at 1200 UTC 11 September with the same initial conditions as used in (a).

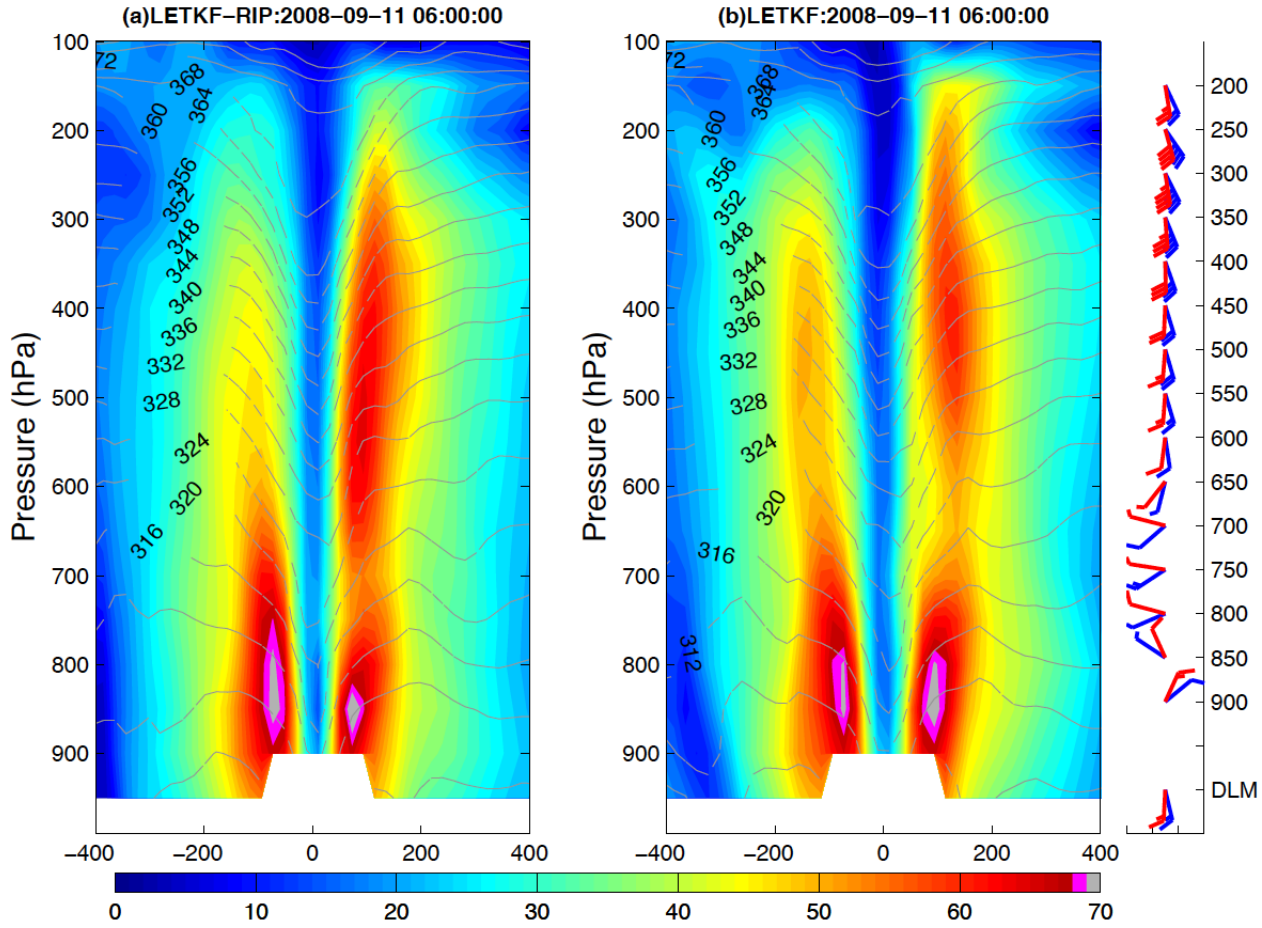

Figure 9 East-west cross section of the typhoon vertical structure from the 2-day forecasts initialized by: (a) the LETKF-RIP and (b) the LETKF analyses at 0600 UTC 9 September 2008. The color shading denotes the wind speed and the contours denote the potential temperature. The blue (red) wind bars on the right-hand side denote the steering flow for the typhoon in the LETKF (LETKF-RIP) forecast in the vertical, and those at the bottom are the deep layer mean wind.

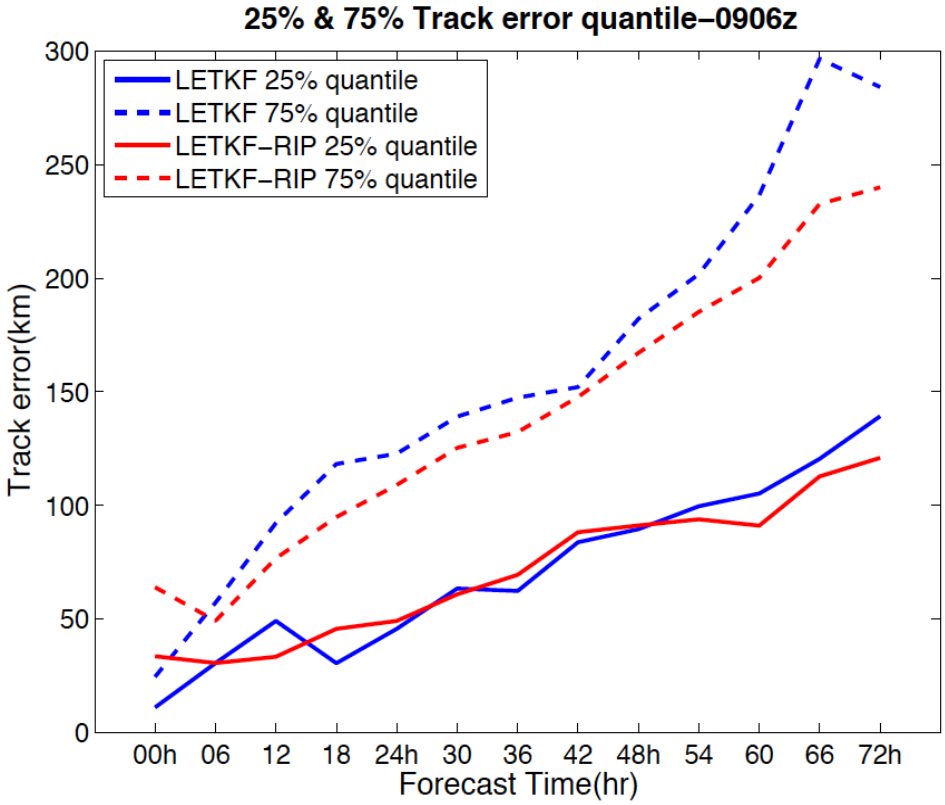

Figure 10 The 25% and 75% quantiles of the ensemble track errors from the LETKF and LETKF-RIP ensemble forecasts initialized at 0600 UTC 9 September.

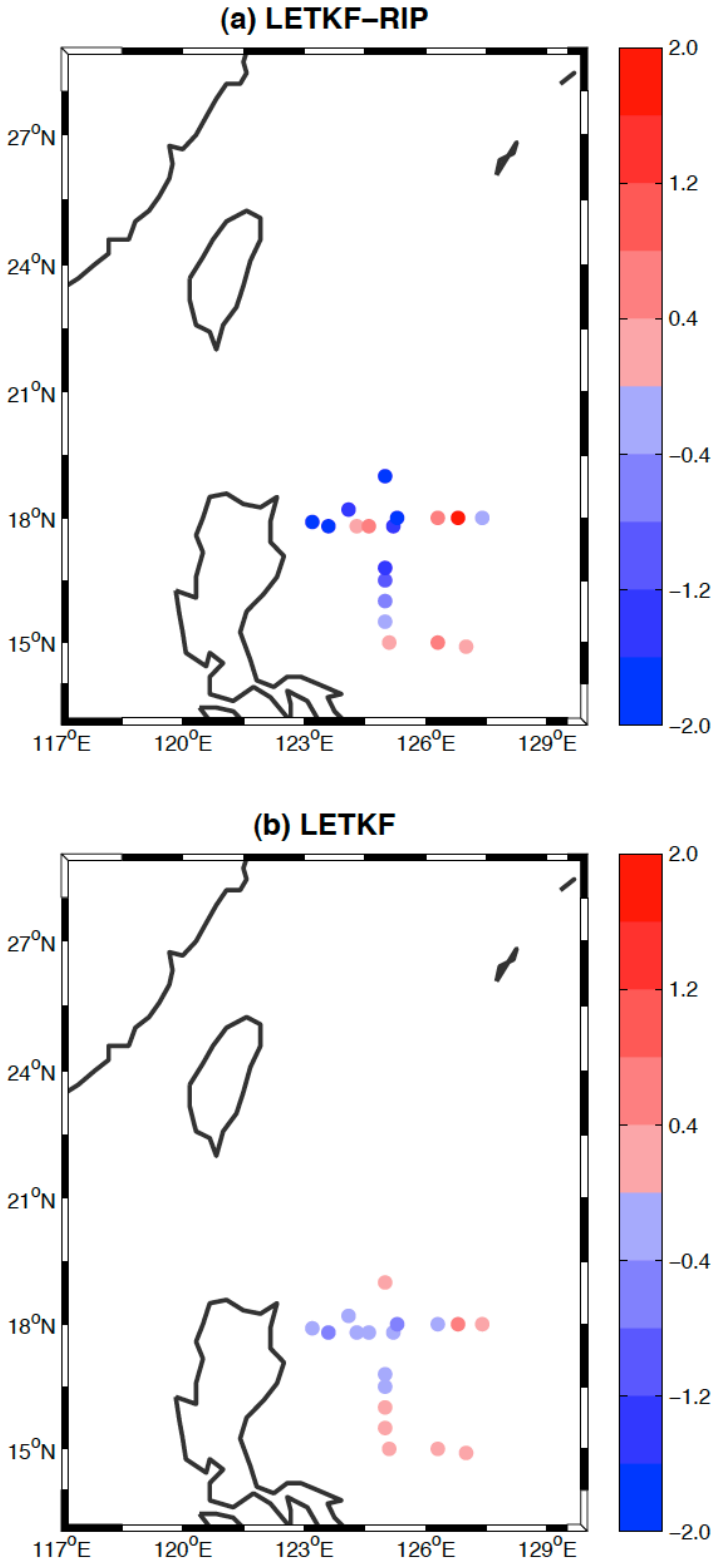

Figure 11 Forecast sensitivity verified at 0600 UTC 11 September with respect to the dropsondes at 0600 UTC 9 September with results of the (a) LETKF-RIP and (b) LETKF analyses and forecasts.

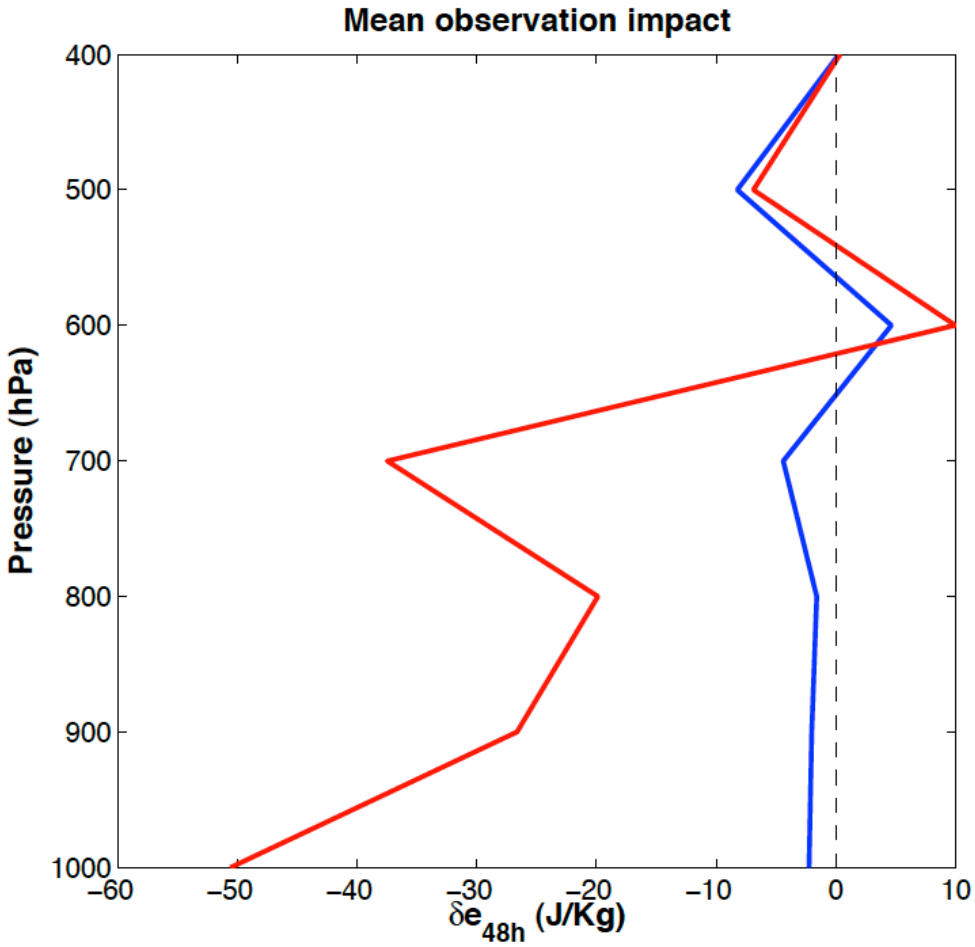

Figure 12 Vertical distribution of the observation impact per dropsonde. The red line denotes the results obtained with the LETKF-RIP experiment and the blue line denotes the LETKF results.

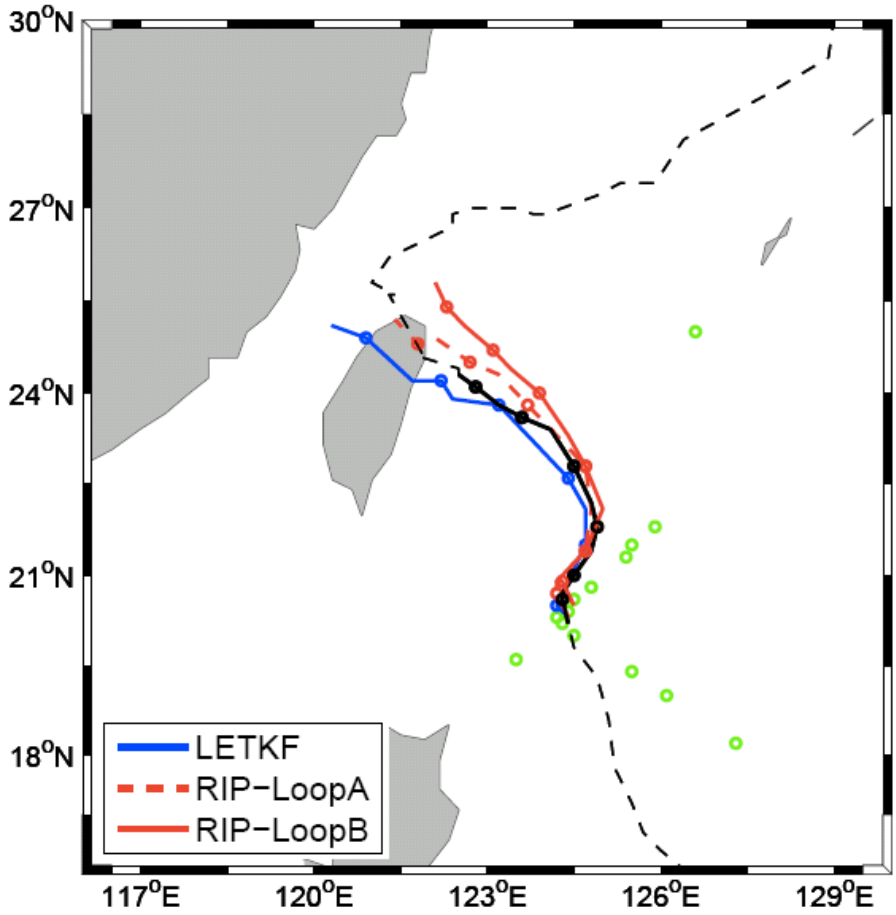

Figure 13 Typhoon track prediction initialized at 0600 UTC 10 September with the LETKF (blue) and LETKF-RIP analysis from Loop A (red dashed line, also the first iteration) and from Loop B (red solid line, also the second iteration). Green dots are the locations of the dropsondes.

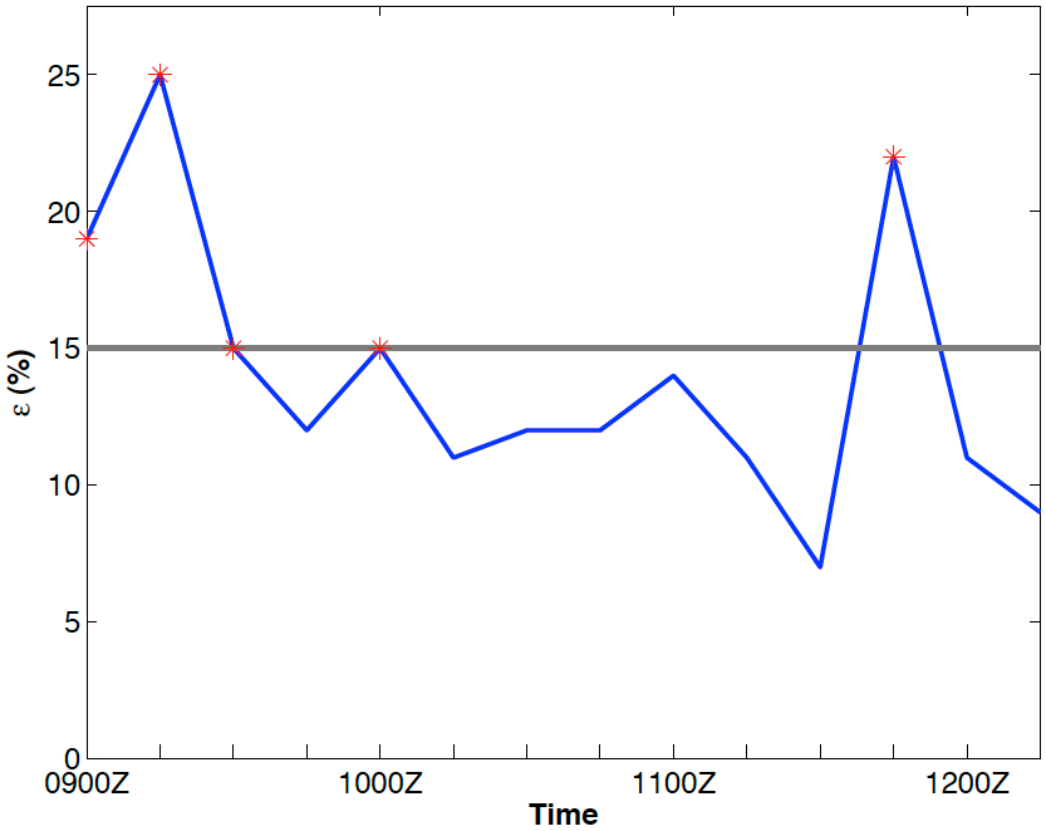

Figure 14 Time series of the ratio ε. The grey line indicates the stopping criterion (15%) to automatically switch the RIP iterations on ($\varepsilon > 15\%$) or off.

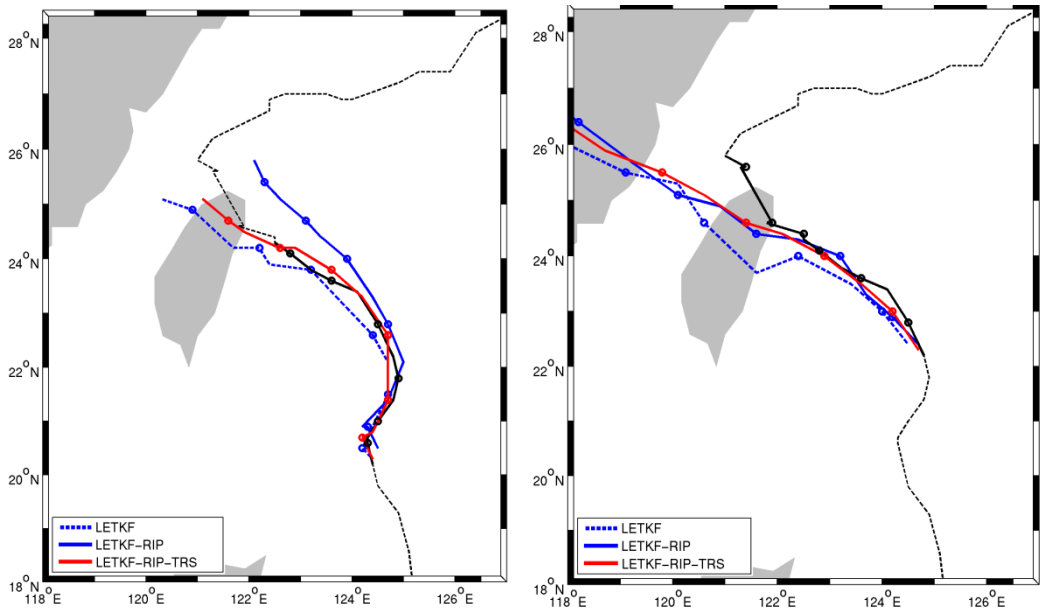

Figure 15 (a) Typhoon track prediction initialized at 0600 UTC 10 September 10 with the LETKF (blue dashed line), LETKF-RIP analysis (blue solid line), and LETKF-RIP-THS analysis (red solid line). (b) Same as (a) except the initial time is 1800 UTC 11 September.

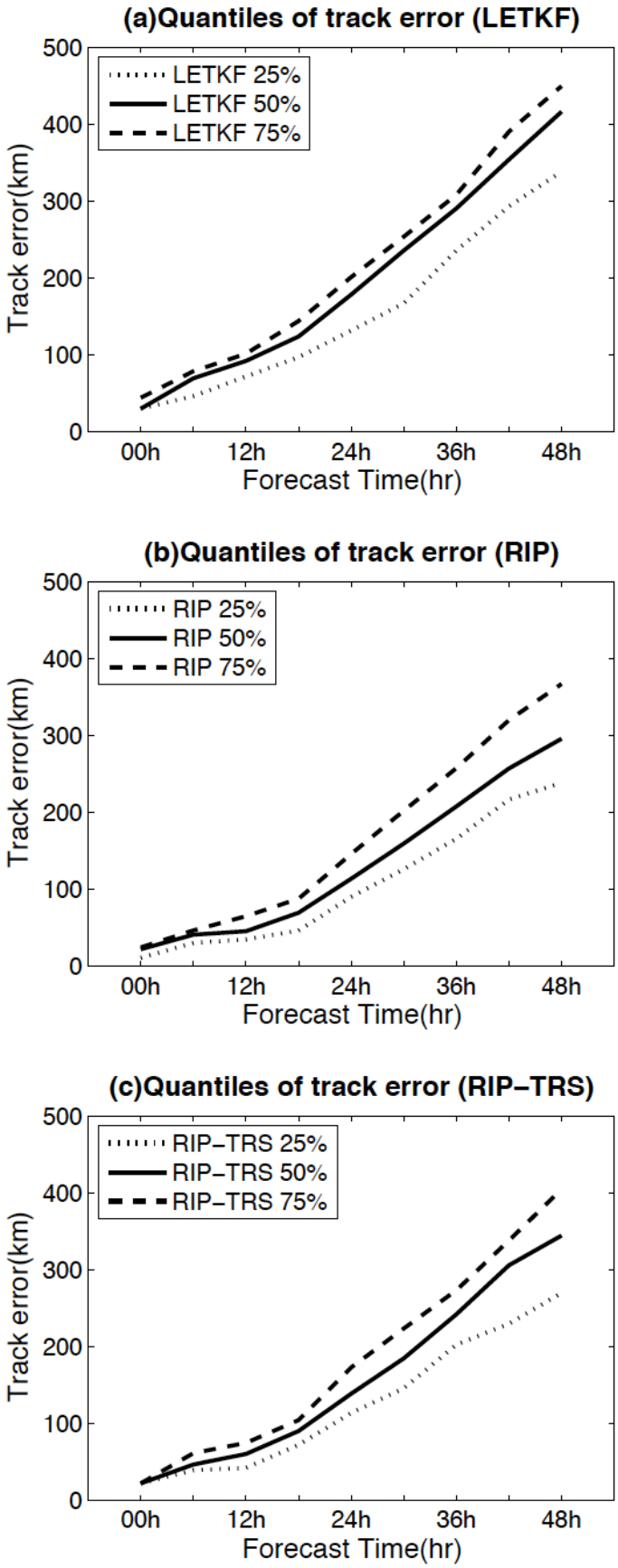

Figure 16 The 25%, 50% and 75% quantiles of the ensemble track errors from: (a) the LETKF, (b) LETKF-RIP and (c) LETKF-RIP-TRS ensemble forecasts initialized at 1800 UTC 11 September.

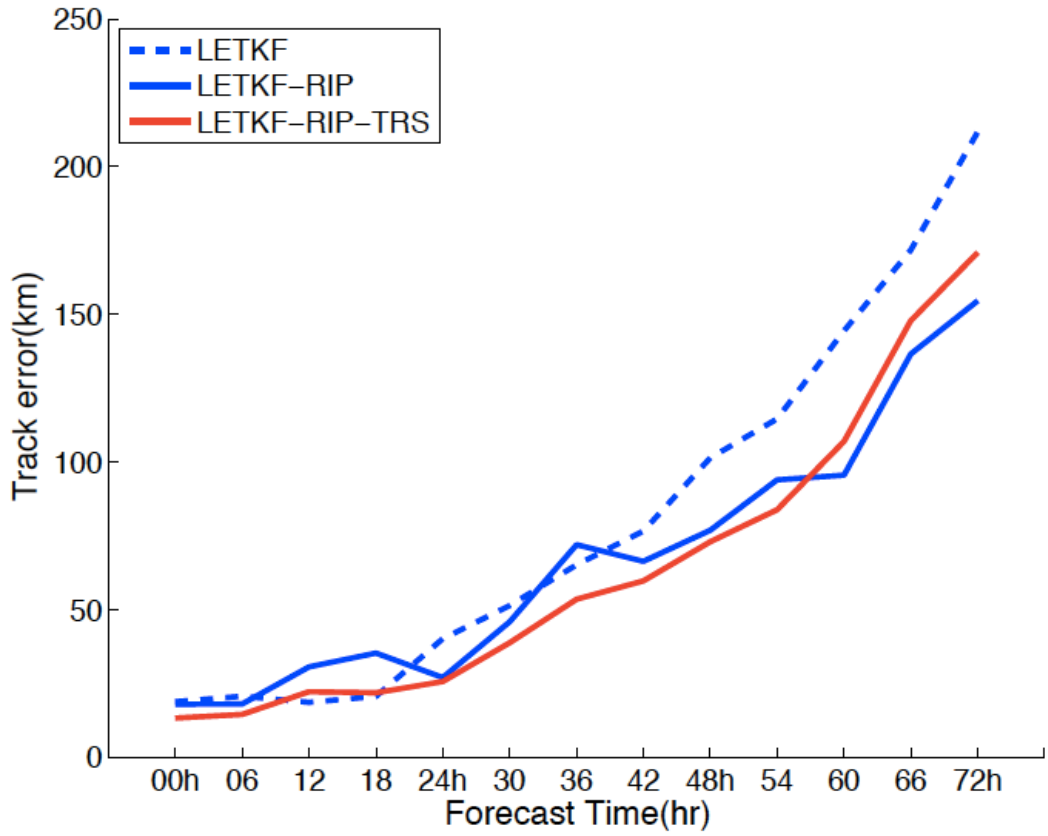

Figure 17 Mean cross track error from the LETKF and LETKF-RIP forecasts at different forecast hours averaged from the cases initialized at 0000 UTC 9 September to 0600 UTC 12 September with a 6-h interval.